

SOLAR WIND INTERACTIONS AND THE MAGNETOSPHERE

A. J. DESSLER

1. The Solar Wind

A. INTRODUCTION

Before undertaking our examination and description of the magnetosphere, we shall discuss the solar wind. We do this because the solar wind is the dominant force on the outer surface of the magnetosphere and presumably is the source of energy for processes occurring within the magnetosphere as well as terrestrial observable events.

As the lectures evolve it will become apparent that the mechanism for coupling the solar-wind energy to the magnetosphere is as yet unresolved; whereas the physical principles governing solar-wind flow are well established and understood (PARKER, 1963).

B. HISTORICAL BACKGROUND

The historical development of the concept of the solar wind is interesting and instructive. The inception of the idea that matter is emitted from the sun, travels through interplanetary space, impinges on the earth's upper atmosphere, and produces a variety of terrestrial phenomena occurred almost simultaneously with the discovery of the gaseous discharge tube. In the 1890's, the analogy between the laboratory experiments with a Crookes tube and auroral phenomena was immediately obvious to Danish and Norwegian scientists, and they concluded that the aurora was a form of cathode rays.

BIRKELAND (1896) was the real pioneer in this area of research. He employed laboratory experiments to support his ideas while others simply made qualitative suggestions. From his terrella experiments he noted that cathode rays were absorbed mainly in the polar regions of the dipole field, and so was able to explain why auroras were observed at the high Norwegian latitudes rather than lower latitudes.

This fruitful line of research was virtually extinguished by KELVIN (1892). In his address to the Royal Society he claimed that the correlation between solar and terrestrial phenomena was merely a statistical 'fluke'. Indeed he stated categorically that there was no connection between the sun and aurora, and between sunspots and magnetic storms. It remained for CHAPMAN (1918, 1919), two decades later, to reinstate the appropriate line of geomagnetic research in England.

The hypothesis had been advanced that comet tails were caused by solar electromagnetic radiation pressure. At the turn of the century FITZGERALD (1900), from his observations that stars were visible through comet tails, argued that such a tenuous gas could not absorb sufficient electromagnetic radiation to account for the observed accelerations. He concluded that some mechanism other than radiation pressure produced this effect. From the calculations of oscillator strength for resonance

absorption, WURM (1943) came to the same conclusion. In a series of papers, BIERMAN (1951, 1953, 1957) postulated that the unknown mechanism was a continuous flow of corpuscular radiation from the sun. Bierman was able to explain the streaming away of comet tails from the sun as a consequence of this flow.

In 1958 Parker proposed that Bierman's continuous flow could be accounted for by a hydrodynamic expansion of the solar corona (PARKER, 1958). The existence of the solar wind is now so firmly established that it is difficult to believe, in retrospect, that it was ever questioned. It was challenged on theoretical grounds by CHAMBERLAIN (1960). He disagreed with Parker's premise that the particles were strongly interacting and so could be treated as a fluid, and later correctly argued that a supersonic hydrodynamic solution was not unique. Thus a spirited controversy arose regarding the exact nature of the expansion of the solar corona.

More than 2 years passed before the first, tentative, direct observations of the solar wind were reported. In 1960, sensors on Lunik 2, Lunik 3, and Explorer 10 collected the first experimental data which corroborated the validity of Parker's model. However, these short-term (~ 1 day) data were not regarded as definitive. It was not until late in 1962, when Mariner 2 results were reported, that the existence of the solar wind was accepted widely.

C. HYDRODYNAMIC EXPANSION OF THE SOLAR CORONA

We now turn to the problem, 'How does an envelope of gas expand around stars?' As we have inferred there are two solutions to this problem, the hydrodynamic solution of Parker and the evaporative solution of Chamberlain (PARKER, 1958; CHAMBERLAIN, 1960). As you may know, the subsonic solution of Chamberlain explains the escape of neutral hydrogen from the geocorona; whereas Parker's subsonic to supersonic solutions explains the flow of particles from the solar corona.

We shall talk first about the basic principles of supersonic flow and then observe that the sun can mock a rocket engine (see, e.g., PARKER, 1963; DESSLER, 1967). Essentially what happens is that the sun behaves like a rocket engine blasting its exhaust into space. In proceeding in this manner, we are guided by the work of Francis Clauser, who was the first to recognize that the hydrodynamic equations describing the expansion of the solar corona are similar to those describing the flow of gas through a deLaval nozzle (CLAUSER, 1960).

How is supersonic flow achieved in a nozzle? If we force gas through a converging nozzle, the flow is choked at the narrowest end (see Figure 1a). No matter what the pressure differential between the ends is or even if the narrow end exhausts into a vacuum, supersonic flow cannot result. The maximum speed of the flow, depending on the pressure differential, developed at the narrowest part is equal to or less than the speed of sound.

The only way to attain supersonic flow in the steady state is by employing a converging-diverging nozzle (Figure 1b). Whether or not supersonic flow is realized depends, of course, on the pressure differential.

A final case, shown as Figure 1c, is the diverging nozzle. The flow in a diverging

nozzle is subsonic. This system is analogous to solar coronal expansion when gravitational effects are neglected.

To demonstrate these qualitative remarks, consider a compressible gas flowing down a tube with variable cross-sectional area. In the steady state, conservation of mass flow requires that

$$s\rho V = \text{const.}, \quad (1)$$

where s is the cross-sectional area, ρ is the mass density, and V is the flow velocity.

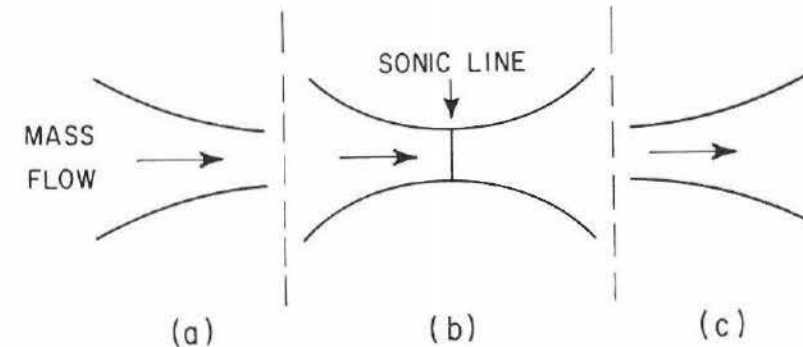


Fig. 1. Nozzle configurations: (a) Converging, (b) Converging-diverging, (c) Diverging.

There is a pressure and velocity differential between the ends. Since the pressure differential is balanced by a time rate of change of momentum, we have, for a tube of unit cross-sectional area,

$$dP = -\rho V dV. \quad (2)$$

It should be noted that dissipative effects, such as viscous and magnetic forces, have been neglected and we are assuming an ideal fluid.

Taking the natural logarithm and total differential of Equation (1), we obtain

$$\frac{ds}{s} + \frac{d\rho}{\rho} + \frac{dV}{V} = 0. \quad (3)$$

We rewrite Equation (2) as

$$\frac{dP}{\rho} = \frac{dP}{d\rho} \frac{d\rho}{\rho} = -V dV.$$

For an adiabatic or isothermal process, we have for the speed of sound, $C_s^2 = dP/d\rho$ or $(C_s^2/\gamma) = dP/d\rho$, respectively, where γ is the ratio of specific heats. Close to the sun, the process is nearly isothermal; at larger distances the adiabatic approximation is preferable. At any rate, the speed of sound is somewhere between these limits, and we can be off by no more than a factor of 5/3 in the square of the speed of sound if we assume an adiabatic process. Thus the above equation becomes

$$d\rho/\rho = -(V/C_s^2) dV. \quad (4)$$

Substituting this result into Equation (3) yields

$$ds/s = [(V/C_s)^2 - 1] (dV/V). \quad (5)$$

Using this basic result, we can now prove our earlier assertions.

Consider a subsonic mass flow ($V < C_s$) in the converging nozzle shown in Figure 1a. Then the bracket $[(V/C_s)^2 - 1] < 0$ and since the cross-sectional area is decreasing ($ds < 0$), in the direction of flow (positive sense), it follows that $dV > 0$, i.e., the velocity is increasing. Since $(dV/V) > 0$ and $(ds/s) < 0$, then V is always less than C_s . This result is independent of anything that you might do to the system. If you were to heat the system internally, C_s and V would change but the sign of the bracket would not.

Next let us examine the converging-diverging nozzle (Figure 1b). Again the flow is initially subsonic and, as before, we have $V < C_s$, $(ds/s) < 0$ and $(dV/V) > 0$. As we proceed in the direction of flow, we arrive at a position where the tube stops converging. Here, the walls are parallel and $ds = 0$. This condition is satisfied if either the bracket or $dV = 0$. The bracket is zero when $V = C_s$ and this condition defines the sonic line shown in Figure 1b. If V is to exceed C_s beyond this line the tube must diverge ($ds > 0$). This configuration is called the deLaval nozzle.

If, on the other hand, the flow is initially so slow that although V is increasing, it remains less than C_s , in the narrowest part of the tube, the condition $ds = 0$ is satisfied by $dV = 0$, and we have the Venturi tube. Now, as we proceed into the diverging section of the tube ($ds > 0$), the equality in Equation (5) is preserved by requiring that the flow slow down again ($dV < 0$).

Finally let us examine Figure 1c, a configuration that we shall return to in our discussion of the sun's expansion. Here, if we start with a subsonic flow, the bracket is negative. Since $ds > 0$ everywhere in this diverging section, dV is always decreasing. Even if this tube were to open into a vacuum, supersonic flow cannot be achieved.

Let us now consider the sun. Clearly we are going to use the deLaval nozzle (Figure 1b) to explain Parker's subsonic-supersonic expansion and the diverging nozzle to examine Chamberlain's subsonic flow. As we remarked earlier, the flow through a diverging nozzle (Figure 1c) is analogous to the escape of particles from the sun when gravity is neglected. If we assume that the particles escape so that we have spherical symmetry, i.e., $s \propto r^2$, where r is the heliocentric distance, we have $ds/s = 2dr/r$. Then Equation (5) becomes

$$2dr/r = [(V/C_s)^2 - 1] (dV/V).$$

With V initially less than C_s and $(dr/r) > 0$, it follows that $dV < 0$ and we see that the flow velocity is always subsonic. This corresponds to a high-temperature limit for the evaporative solution of Chamberlain.

Let us now include the effects of the sun's gravitational force. Newton's second law, Equation (2), becomes

$$dP = -\rho V dV - \rho M_\odot G dr/r^2, \quad (6)$$

where M_\odot is the solar mass, and G is the gravitational constant.

Using Equation (6) and proceeding as before we have

$$ds/s = [(V/C_s)^2 - 1] (dV/V) + (M_\odot G/C_s^2 r) (dr/r).$$

In order to continue, we must again an assumption about the flow tube. We shall assume spherical symmetry, although we could equally well assume any power law, $s \propto r^n$. However, this is not a critical assumption and spherical symmetry works well. The above equation becomes

$$[2 - (M_\odot G/C_s^2 r)] (dr/r) = [(V/C_s)^2 - 1] (dV/V). \quad (7)$$

This is the fundamental equation.

If the coronal gas velocity increases monotonically outward ($dV > 0$ and $dr > 0$) and initially is subsonic, then the heliocentric distances for subsonic and supersonic flow are given by

$$M_\odot G/C_s^2 r > 2 \quad \text{and} \\ M_\odot G/C_s^2 r < 2, \quad \text{respectively.}$$

The flow reaches sonic velocity at the critical radius

$$r_c = M_\odot G/2C_s^2. \quad (8)$$

The sonic velocity for ionized hydrogen is given by $C_s^2 = 2kT\gamma/m$ (assuming thermal equilibrium between electrons and protons) where m is the proton mass. Using this relation we can write the critical radius in terms of well-known constants

$$r_c = [M_\odot m G/4\gamma k T_c]. \quad (9)$$

The sun's gravitational force has had the effect of changing the nozzle representation from a diverging system to a converging-diverging system.

Knowing the temperature of the solar corona we are now able to estimate the critical radius. For $T \sim 2(10)^6$ K, $r_c \sim 1.7 R_\odot$, where R_\odot is the solar radius. The maximum temperature at which supersonic expansion can occur is determined by setting $r_c = R_\odot$ in Equation (9). This yields $T_{\max} \sim 4(10)^6$ K. For the sun the coronal expansion will always be supersonic because the relatively low temperatures in the chromosphere are available to insure $r_c > R_\odot$.

Supersonic expansion occurs only over a limited range of coronal temperatures. If the corona is too cool, the atmosphere is essentially static and no significant flux will result. If the sun and corona (and chromosphere) are too hot ($T \gtrsim 4(10)^6$ K) the expansion will take place at entirely subsonic speeds.

To amplify slightly on this last point consider an extended but non-expanding atmosphere with no exosphere. The density is given by

$$\rho(r) = \rho_0 e^{-r/H}, \quad (10)$$

where $H = kT/mg$ is the scale height. If the atmosphere is heated and begins to expand and escape into space, the mass flow through any spherical surface is

$$4\pi\rho(r) V_r r^2 = \text{const.} \quad (11)$$

If the temperature is very high, then from Equation (10) we see that $\rho \approx \rho_0$ and from Equation (11) we have $V_r \propto 1/r^2$. In this case, the flow velocity decreases monotonically, which corresponds to the diverging nozzle configuration. If, on the other hand, the temperature of the atmosphere is cooler, ρ decreases sharply, and V_r must increase to keep the mass flow constant. At some heliocentric distance V_r will reach the speed of sound. Additional expansion beyond this point will lead to supersonic flow. Thus we conclude that the role of gravity in supersonic expansion is to cause the mass density to decrease more rapidly than $1/r^2$.

D. RESOLUTION OF THE PARKER-CHAMBERLAIN CONTROVERSY

We are now in a position to understand the difference between the hydrodynamic solution of Parker and the evaporative solution of Chamberlain. First let us note that both solutions are correct, but they apply to different boundary conditions. Parker's solution pertains to a cool but not too cool corona; whereas Chamberlain's solution is valid in coronal regions close to the star and for $T > T_{\max}$.

The evaporative solution applies to an exosphere where particles can move beyond some critical distance r_0 only by traveling along ballistic trajectories. Escaping particles move along hyperbolic orbits, and non-escaping particles move along elliptic orbits. Only a small fraction of the particles can escape. At radial distances not too far above the exosphere, the velocity-distribution function is essentially Maxwellian. Thus near the star and for sufficiently hot stars ($T > T_{\max}$), both solutions are compatible. However, where $r \gg r_0$, the evaporative model shows an anisotropic temperature in contrast with the isotropic temperature of the hydrodynamic model. Thus, we must expect different results at large distances.

To see why the evaporative model always leads to subsonic solutions, we note that $\rho(r)$ appearing in Equation (10) should be applied to the escaping particles. Since they represent the high end of the thermal distribution, we see that $\rho(r)$ decreases very slowly with heliocentric distance. Thus from Equation (11), it follows that V_r must decrease with r . Thus, sonic and supersonic flow are never achieved in the evaporative model.

In summary, the resolution of the Parker-Chamberlain controversy is as follows: In the evaporative approximation to the behavior of the solar corona, the assumption of no collisions beyond the exosphere precludes the possibility of the outer corona being accelerated to sonic velocity by the expansion of the inner corona. The effect of collisions in the hydrodynamic model is to permit the corona to expand as a whole.

2. The deLaval Nozzle Analogy for the Solar Wind

The deLaval nozzle forms the basis for a rocket engine (Figure 2). For an ideal gas in the combustion chamber at temperature T_c , the maximum exhaust velocity is $V = 3^{1/2} C_s = \gamma^{1/2} v_{r.m.s.}$, where $v_{r.m.s.}$ is the root mean square speed of the gas atoms in the combustion chamber (DESSLER, 1967). Here the rocket engine converts the disordered thermal motion in the combustion chamber to ordered streaming motion.

There is no magic in this, i.e., you do not get something for nothing. The streaming velocity is determined by the combustion-chamber temperature and not the pressure. To an observer in a frame of reference moving with the gas, the supersonic streaming gas is relatively cool. Beyond the sonic line, higher velocities can be achieved by heating the gas which has started to cool by expansion. This is the principle of the jet engine afterburner.

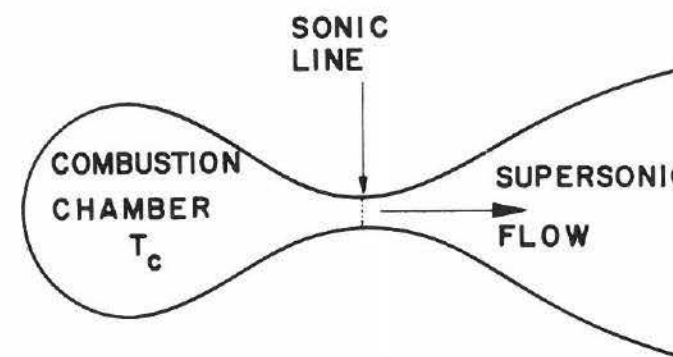


Fig. 2. The converging-diverging nozzle operating as a deLaval nozzle forms the basis for a rocket engine.

In a similar manner, expansion beyond the critical heliocentric distance, r_c , in supersonic flow leads to conversion of thermal energy into streaming energy. The application of heat beyond r_c adds additional thermal energy that later can be converted into streaming energy. Once supersonic flow is established, we can account for any solar-wind velocity simply by heating the supersonic gas.

A. THERMAL STRUCTURE OF THE SUN

Let us now briefly discuss the thermal structure of the sun. The temperature profile of the sun between the photosphere and inner corona is roughly as shown in Figure 3. The sun has a high temperature inside, and by conduction heat is carried out to the photosphere. The visible surface is at $6(10)^3$ °K. Above this surface there is a temperature minimum due to loss of heat by radiation from the chromosphere.

The corona is heated beyond what one would expect simply from thermal contact with the photosphere. This additional heat is thought to be supplied by the dissipation of wave energy generated at the photosphere (BIERMAN, 1946; ALFVÉN, 1947). Both magneto-acoustic and internal gravity waves have been suggested. The argument advanced goes as follows: the relative pressure amplitude $\Delta P/P$ is less than one in the chromosphere and so the waves pass through this region without loss of energy. In the corona, ΔP remains relatively constant whereas P decreases. In this region $\Delta P/P > 1$ and shock waves form. Now the ordered wave energy is converted into thermal energy that maintains the coronal temperature at $(1-2)(10)^6$ °K.

Even if the temperature in the corona were to exceed $T_{\max} \sim 4(10)^6$ °K, we would still have supersonic flow. Somewhere in the relatively cooler chromosphere or

photosphere we would find a self-consistent r_c and T_c , where the transition from subsonic to supersonic flow could occur.

While we are discussing solar temperatures, let us consider two hydrodynamic solutions that give subsonic flow. One such solution occurs when $T < T_m$ and decreases with heliocentric distance as $1/r$. In this case, the critical radius is at infinity. From Equation (9) we can see that r_c is always greater than any given r , so we never reach the throat. Another special subsonic solution occurs when the gas passes through the throat with a velocity that is less than the speed of sound. Equation (7) can be satisfied at the critical radius if $dV=0$ rather than $[(V/C_s)^2 - 1]=0$. This solution corresponds to the flow through a Venturi tube.

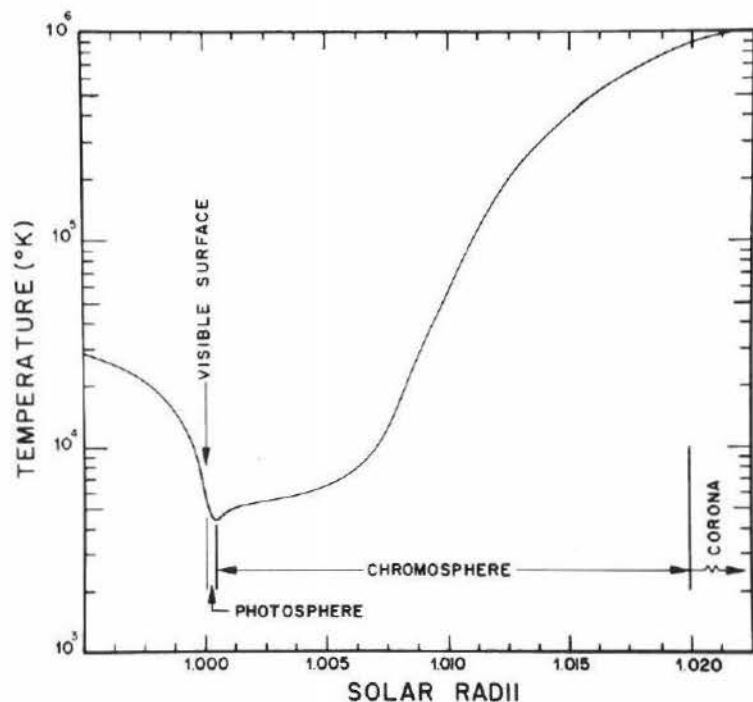


Fig. 3. The temperature profile of the sun.

B. SOLAR MAGNETIC FIELD

Parker and Chamberlain explicitly neglected the effect of the sun's magnetic field in their hydrodynamic and evaporative solutions, respectively. Nevertheless, it is because there is a solar magnetic field that the ordinary hydrodynamic equations are appropriate. Parker assumed that for the solar corona, the collision mean free path (λ) is less than the local scale height H . In Chamberlain's early analysis, λ was greater than H and an exosphere was defined. For the sun, the heliocentric distance to this point where $\lambda \approx H$ is between 2 and $3R_\odot$ depending on the temperature used. Beyond this distance, the hydrodynamic equations should be inappropriate. But we are assured by

its success that the hydrodynamic approximation is valid beyond this distance.

To resolve this apparent dilemma, let us speculate qualitatively on the role of the solar magnetic field in producing collisions which randomize the particle velocity. Let us postulate 'magnetic collisions' that produce strong particle interactions. A charged particle spiraling in a magnetic field produces a fluctuating current that has an external magnetic field that fluctuates at the cyclotron frequency. This field acts on nearby particles while their fields, in turn, act on the initially singled out particle. (Note that particles of like mass have identical cyclotron frequencies.) Such interactions between particles could conceivably couple them so that there is no exosphere for the corona.

Once we agree to treat the corona as a continuum, we must account for the energy in the supersonic flow. To get a feel for the magnitudes involved let us use some representative numbers. Assume that at the base of the corona the protons and electrons each have 100 eV of thermal energy. This corresponds to a temperature, $T \sim 1.16(10)^6$ °K. At the earth's orbit, protons are observed having an energy of ~ 1.1 keV corresponding to $V_s \sim 4.5(10)^2$ km/sec. The total energy of the electrons is negligible (~ 25 eV). The work done against gravity in bringing a proton-electron pair from the base of the corona to 1 AU is 2 keV. Thus each proton-electron pair arrives at the orbit of the earth with a kinetic plus potential energy of 3.1 keV/pair. The energy available at the base of the corona is 0.3 keV. This means that 2.8 keV/pair must be supplied by extended coronal heating. There are several methods for adding energy to the moving gas. One method is thermal conduction by electrons; the other as we mentioned, is by shock-waves propagating from the sun.

What is the effect of solar rotation on the solar wind? Assume that the solar gas is emitted radially from a small area near the solar equator with constant velocity. Looking down on the equatorial plane, we can watch the flow of the gas for several days. Figure 4 can be interpreted as a picture taken on the sixth day and the numbers indicate the day of emission. Although each element of gas moves radially (or very nearly so), the sun's rotation produces a curved particle stream (Archimedean spiral). This picture was first described by Chapman in his analogy with a stream of water coming from a garden hose (CHAPMAN, 1929). It is the origin of the term 'garden-

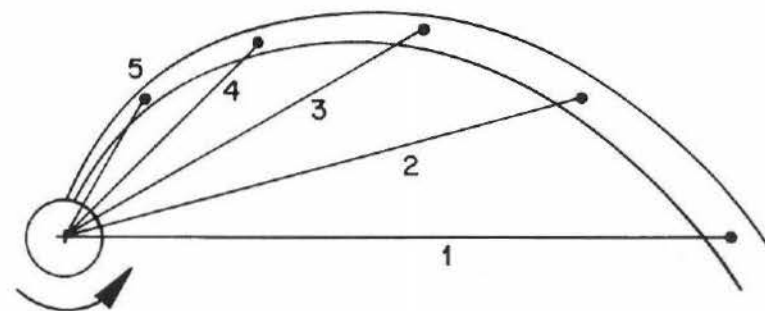


Fig. 4. The formation of the Archimedean spiral by the solar wind.

hose angle' that is often used to name the angle between the radius vector and the local tangent to the Archimedean spiral.

Since we have a very highly conducting plasma the lines of force are 'frozen into it'. They must follow the particle stream line and so form Archimedean spirals (Figure 5). The field, for large r , in the equatorial plane is given by

$$\begin{aligned} B_t &= B_0 (b/r)^2 [1 + (\Omega r/V_s)^2]^{\frac{1}{2}} \\ B_{\parallel} &= B_0 (b/r)^2 \\ B_{\perp} &= B_0 (b^2 \Omega / r V_s), \end{aligned} \quad (12)$$

where B_t is the total field, B_0 is the field strength at the reference distance b , Ω is the angular velocity of the sun, and the symbols \parallel and \perp are with respect to the solar radius vector (PARKER, 1963).

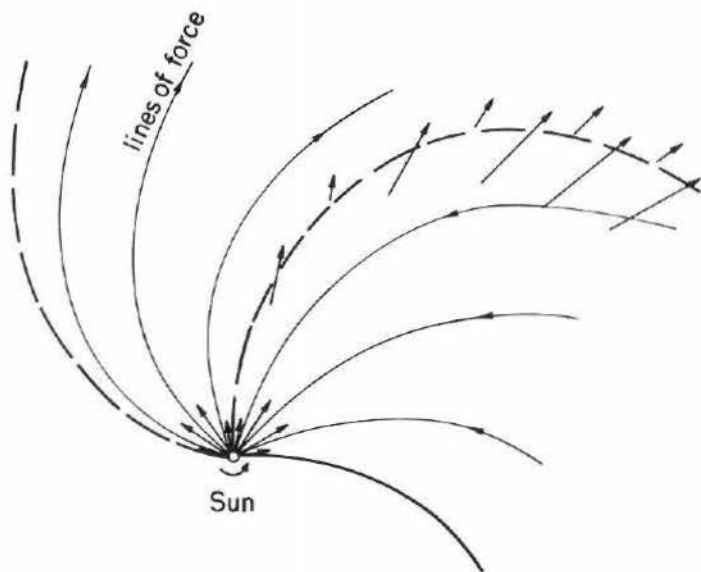


Fig. 5. The magnetic lines of force in the solar equatorial plane forming Archimedean spirals.

Using these equations we can make predictions about the interplanetary magnetic field. For $r > 0.1$ AU they can be evaluated with good accuracy by letting $b = 1 R_{\odot}$, $B_0 \sim 1$ gauss, and having the value for Ω correspond to an equatorial rotation of 24.7 days. The component results are graphed in Figure 6 for three values of V_s . Figure 7 shows the total field for the same three values of V_s and is limited to a range near 1 AU. Over the chosen range of V_s , the magnetic-field strength is a rather sensitive function of V_s .

The predicted results agree quite well with observations. Figure 8 shows the distribution of the interplanetary magnetic-field direction. The histograms show the direction of the magnetic field with respect to the earth-sun line, and with respect to

the ecliptic plane (NESS and WILCOX, 1964). They represent a number of observations using 5.46-min averages of data. If you look at the results in the plane of the ecliptic you see that the field pretty generally points along an Archimedean spiral. Notice also that 48% of the time, the field is pointing away from the sun and 35% of the time it points toward the sun. However, if we examine the histograms for data normal to the plane of the ecliptic, we infer that there is usually a Southward (with respect to the sun's poles) field component.

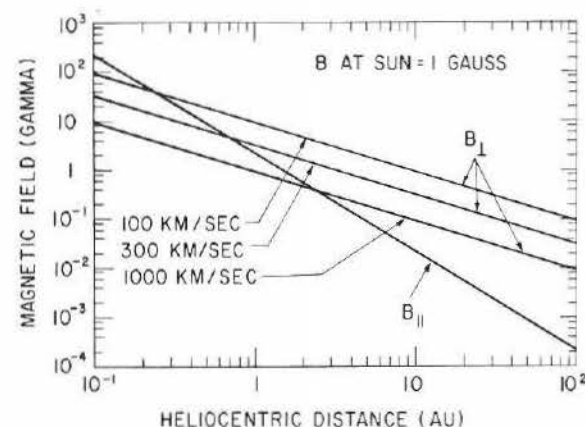


Fig. 6. Values of the parallel (B_{\parallel}) and perpendicular (B_{\perp}) (with respect to the solar radius vector) components of the interplanetary magnetic field.

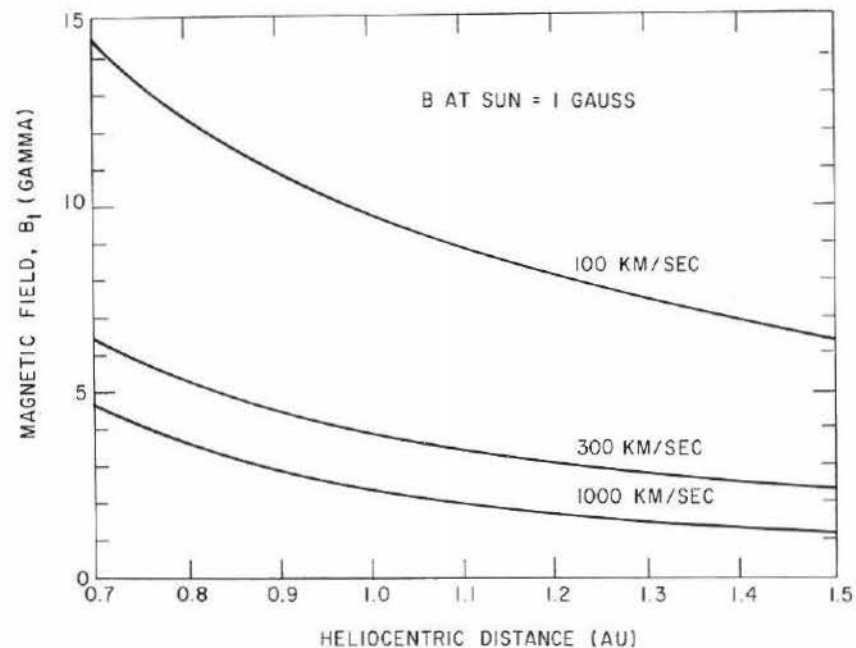


Fig. 7. The variation of the total interplanetary magnetic field with heliocentric distance.

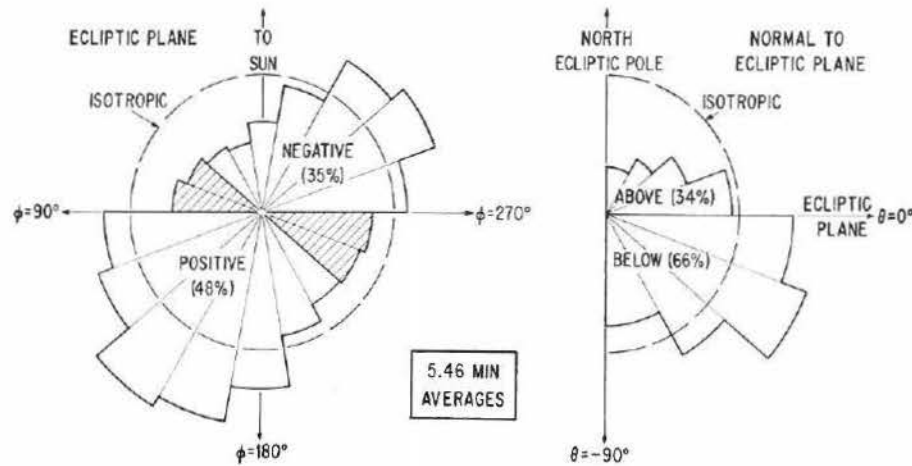


Fig. 8. Distribution of the interplanetary magnetic-field direction.

This Southward directed component represents a serious discrepancy between theory and experiment, since it is, in effect, a field component perpendicular to the ecliptic plane. Measurements made on Mariner 2, IMP I, and Mariner 4 indicate that there is a perpendicular component which has a Southerly sense and a strength of about 1γ ($1 \gamma = (10)^{-9} \text{w/m}^2$) (COLEMAN *et al.*, 1962, 1966; NESS *et al.*, 1964, 1966). Theory, on the other hand, does not predict a latitudinal component, B_θ , although we must admit of the possibility of a transient $\hat{\theta}$ -component due to interplanetary irregularities and fluctuations. These fluctuations would, however, give a zero average for B_θ .

To illustrate the seriousness of this discrepancy let us assume that there is a Southerly perpendicular component, $B_p \sim 1 \gamma$. The solar wind flowing through this field produces an electric field, $\mathbf{E} = -\mathbf{V}_s \times \mathbf{B}_p$. The situation is shown in Figure 9. The net change of flux within the circle of radius r is

$$-\frac{\partial \Phi}{\partial t} = \oint \mathbf{E} \cdot d\mathbf{l} = V_s B_p 2\pi r. \quad (13)$$

Letting $V_s \sim 400 \text{ km/sec}$ and $r \sim 1 \text{ AU}$, the above equation yields

$$\partial \Phi / \partial t \sim 4(10)^8 \text{ w/sec.}$$

In the time for one solar rotation, the magnetic-flux change would be $8(10)^{14} \text{ w}$. If this flux change were to appear in interplanetary space, it would be distributed over the area of a circle of radius 1 AU. This would lead to a change in B_p of more than 10γ . Such a change has not been observed. There are other ways to explain this flux change, but they are equally unsatisfactory.

Let us conclude this discussion by stating that the observed Southward directed perpendicular component may be largely illusory. Magnetic experiments are difficult

to perform, and complete, absolute in-flight calibration of the magnetometers has not been possible to date. The perpendicular component might be simply an experimental error. What is more, recent IMP 3 and Pioneer 6 experiments do not observe this component (NESS, 1966; NESS *et al.*, 1966).

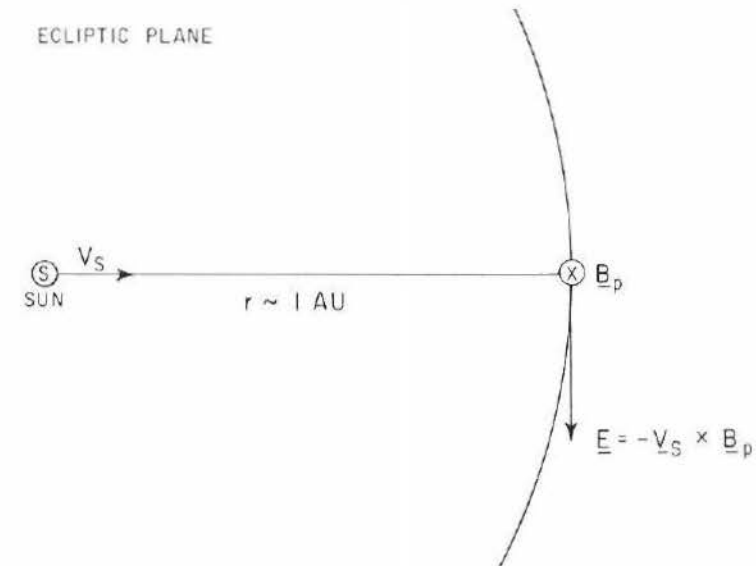


Fig. 9. Schematic representation of the electric field produced by an interplanetary magnetic-field component normal to the ecliptic plane.

Observations by NESS and WILCOX (1965) show that the solar magnetic field has a simple sector-like structure. They observed that the field near the sun's equatorial plane was divided into four sectors, depending on whether the field was predominantly toward or away from the sun. This condition of oppositely directed field lines is shown in Figure 5. The field reverses sharply across each sector boundary to give the next sector of field with opposite sense.

Within a sector, the features as reported by NESS and WILCOX (1965) and WILCOX and NESS (1965) are unexpected and as yet unexplained (see Figure 10). They find that the field strength is not constant within a tube of force but rather tends to follow a regular pattern. It rises to a maximum 2 or 3 days following the leading edge of the flux tube and falls to a minimum in the tube about 5 days later. The solar-wind velocity and density are also asymmetrically distributed within a sector.

It appears that the boundaries separating the adjacent tubes are relatively thin ($\approx (10)^5 \text{ km}$) (WILCOX and NESS, 1965). Further, there does not appear to be any magnetic connection between sectors. Such a region is, of course, ideal for magnetic merging to occur. If merging were to take place according to Sweet's mechanism, the gas would be squeezed out from between the two regions of oppositely directed field, permitting the fields to move together and annihilate themselves (Figure 11a). The

fields would then reconnect between the two regions at the edges of the annihilation as shown in Figure 11a. An alternate way for merging to occur has been proposed by PETSCHER (1964). His method is a modification of Sweet's mechanism. Here, as the plasma is squeezed out, the magnetic field is carried away with it (Figure 11b).

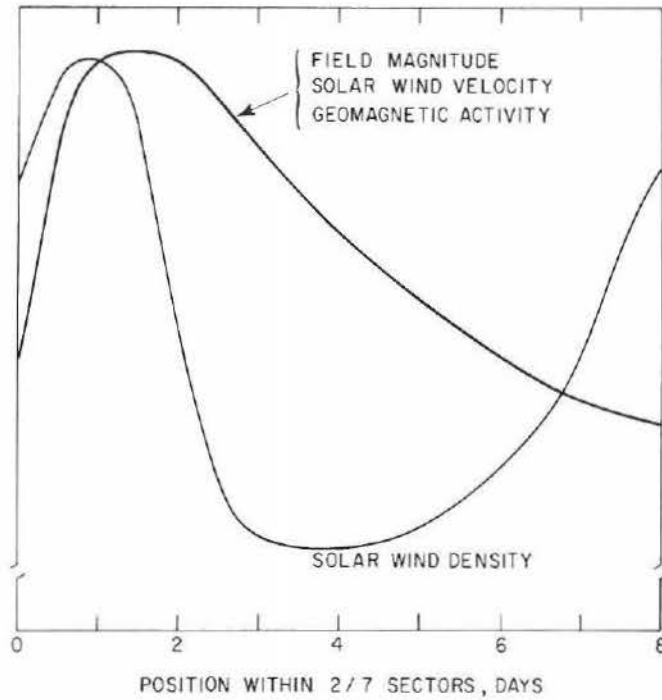


Fig. 10. Schematic representation of the average interplanetary parameters within a solar-sector Structure.

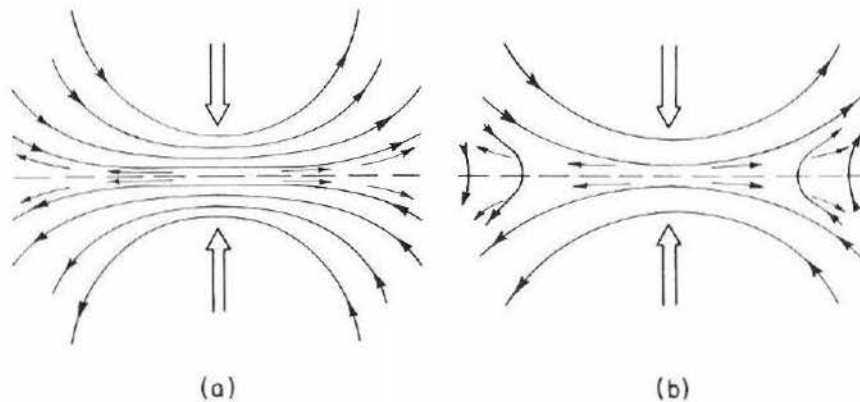


Fig. 11. Merging mechanisms: (a) Sweet's, (b) Petschek's modification of Sweet's.

It takes the solar wind approximately 3 days to travel 1 AU. If fast merging of the types described above occurred, we should expect to see a bubble structure as shown in Figure 12. To date such structure has not been observed. We may therefore conclude that magnetic merging is not a dominant process along sector boundaries.

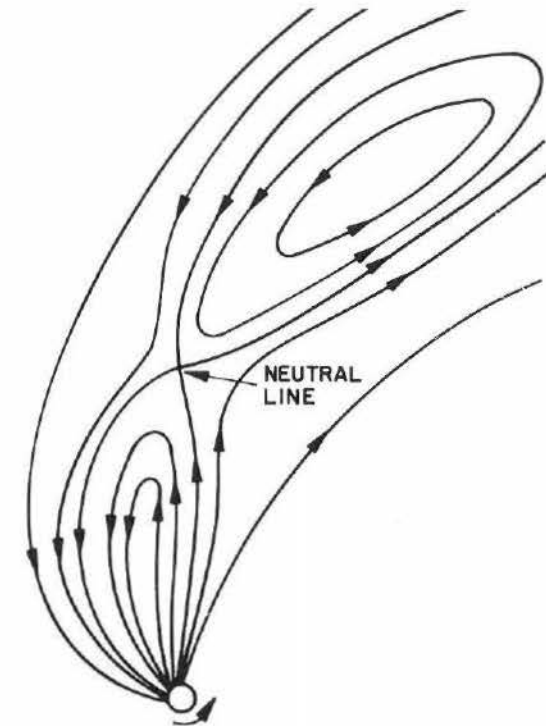


Fig. 12. Sketch showing bubble structure produced by rapid merging between sectors.

C. TERMINATION OF THE SOLAR WIND

Let us now consider the interaction between the solar wind and the interstellar medium. The solar mass density decreases as $1/r^2$, so that the streaming pressure of the solar wind will ultimately become so small that it will be unable to push aside the interstellar medium. First however, as CLAUSER (1960) pointed out, the supersonic solar wind must go through a shock transition before merging with the effectively subsonic interstellar medium.

Figure 13 contains a sketch of a possible interaction configuration. The inner region is called the heliosphere. It is defined as that region of space where the solar wind is flowing supersonically. At some heliocentric distance, r_h , the solar-wind pressure is balanced by the pressure of the interstellar medium. At this distance the solar wind undergoes a shock transition to subsonic flow. The subsonic plasma beyond the shock forms a boundary shell. Beyond the boundary shell lies the interstellar medium.

To estimate the location of the boundary shell, we simply equate the solar-wind momentum with the pressure of the interstellar medium. Then

$$\rho_{s_0} (r_E/r_h)^2 V_S^2 = P_i(r_h), \quad (14)$$

where ρ_{s_0} is the solar-wind mass density at $r_E = 1$ AU and $P_i = (B_i^2/2\mu_0) + \rho_i v_i^2$. Solving for $\xi_h = r_h/r_E$, we have

$$\xi_h = V_S (\rho_{s_0}/P_i)^{1/2}. \quad (15)$$

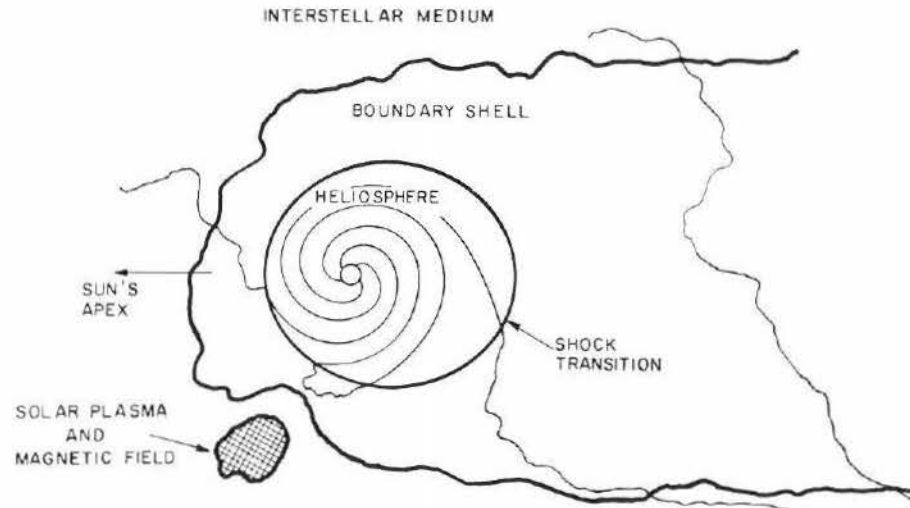
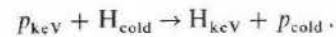


Fig. 13. Illustration of the interaction configuration between the solar wind and the interplanetary medium.

Let $V_S \sim 4(10)^2$ km/sec² and $\rho_{s_0} \sim 8(10)^{-21}$ kg/m³ be the representative numbers for the solar wind. If we assume P_i is due entirely to magnetic field pressure and $B_i \sim 1$ γ , then $\xi_h \sim 60$ or $r_h \sim 60$ AU. This figure is probably a little high. The sun is moving with respect to the interstellar medium with a velocity $v_i \sim 20$ km/sec. If the interstellar medium is composed of neutral hydrogen, $\rho_i \sim 1.7(10)^{-21}$ kg/m³, then P_i is almost tripled and $r_h \sim 30$ AU.

Now if the interstellar medium is, in fact, neutral hydrogen we can expect that as the solar wind streams through it, charge exchange between the solar-wind protons and the interstellar hydrogen will occur.



This would result in an omnidirectional shower of neutral, hot hydrogen atoms. Consequently a useful tool for investigating the boundary shell and the interplanetary medium is the study of the distribution of Lyman α ($L\alpha$) resonantly scattered by atomic hydrogen in interplanetary space (PATTERSON *et al.*, 1963).

D. NON-RADIAL FLOW

Our final topic today is non-radial flow. Thus far we have considered a uniform, spherically symmetric solar wind. Plasma measurements made on Mariner 2 show that the solar-wind velocity varies (NEUGEBAUER and SNYDER, 1966). There are places on the sun where the velocity is high and other places where it is low. This structure can persist for several solar rotations. Suppose, e.g., we observe a solar-wind velocity of 300 km/sec and some 6–10 hours later the speed increased to 500 km/sec. What happens when the fast stream overtakes the slow stream? The fast and slow streams collide and gas from both streams piles up in a growing intermediate region of higher density, pressure, temperature, and magnetic-field strength. Two shocks will be generated if the relative velocity difference between the colliding plasmas is greater than about 100 km/sec. Figure 14 shows the resulting structure under this condition. Notice the arrows showing the solar-wind velocity in the different regions relative to the radius vector.

The shock waves cause the solar wind to be deviated from radial flow owing to the component of flow behind a shock that is perpendicular to the shock front. As the shock passes a stationary observer, the flow is first deviated Eastward between the first shock and the tangential velocity discontinuity and then Westward until the second shock passes. It is this deviation in the solar wind that produces the tangential velocity discontinuity.

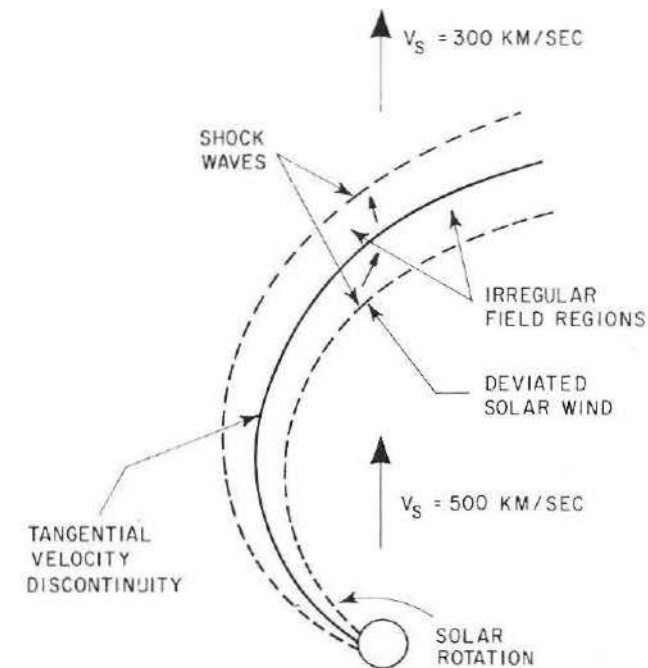


Fig. 14. A projection on the solar equatorial plane showing the interaction between solar winds of different velocities.

Thus we have two hydromagnetic fluids in relative motion. The two fluids will tend to stabilize at the interface unless the magnetic-field lines are parallel or anti-parallel, in which case the interface is unstable for any relative velocity. Since the field lines on either side of the tangential velocity discontinuity are expected to follow the Archimedean spiral, and therefore are parallel, a Kelvin-Helmholtz instability should develop at the interface and generate turbulence.

3. Minimum Stable Solar-Wind Velocity

When the kinetic-energy density of the streaming plasma is much greater than the plasma's magnetic-energy density, the spiral field is carried outward into interplanetary space by the wind. On the other hand, a sufficiently strong solar magnetic field could contain the solar corona so that there would be no solar wind. Alternatively, a very weak solar wind (a solar breeze) would result in a confined corona. To demonstrate this, let us define a quantity β as the ratio of the solar-wind kinetic-energy density to the magnetic-field energy density. Thus

$$\beta = \mu_0(\rho_s V_s^2 + 6nkT)/B_i^2, \quad (16)$$

where n is the proton-number density. Except near the sun, the kinetic-energy density is dominated by the streaming energy. So for a highly supersonic flow $\beta \sim \mu_0 \rho_s V_s^2 / B_i^2$. For large heliocentric distances β is approximately constant since ρ_s and B_i^2 both fall off as $1/r^2$ and V_s is essentially independent of r . The condition for stopping the solar wind is $\beta < 1$ or $B_i^2 / \mu_0 > \rho_s V_s^2$. If we assume that $B_0 \sim 1$ gauss in the expression $B_i^2 \sim B_0^2 (R_0^4 / r^2) (\Omega / V_s)^2$, and $n \sim 10/\text{cm}^3$, it is easily shown that for $V_s < 100$ km/sec, the interplanetary field would be spiraled so tightly as to prevent flow. It is clear that this condition precludes our acceptance of a solar-breeze solution where $V_s \sim 20$ km/sec.

THE MAGNETOSPHERE

1. Introduction

We are now ready to examine the interaction between the solar wind and the geomagnetic field. The word 'magnetosphere' was first used by GOLD (1959). It is that volume of space surrounding the earth where the motion of charged particles is largely governed by the geomagnetic field. Its inner boundary is in the E-region of the ionosphere at an altitude of about 150 km. Its outer boundary is variable and complicated and has a minimum and maximum length along the earth-sun line. In the solar direction, the distance is about $10 R_E$; in the anti-solar direction the length is unknown and estimates range from hundreds of earth radii to astronomical units.

CHAPMAN and FERRARO (1931, 1940), in their study of magnetic storms, constructed a model wherein the geomagnetic field was confined to a cavity during disturbed times. Hoyle and Dungey independently postulated that the earth's field was confined by the orbital motion of the earth through a static solar corona. These models were constructed in pre-solar wind days and made use of the earth's orbital

motion through a static corona. The ideas about confinement changed markedly with the advent of Parker's solar-wind theory. Parker suggested that a continuous solar wind implied a continuous confinement. The confining flow was no longer considered to be in the direction of the earth's orbital velocity vector but rather in a radial direction outward from the sun.

2. Models

It was expected on the basis of theoretical arguments that the solar wind would distort the geomagnetic field asymmetrically. Depending on the initial assumptions, the models varied. One of the earliest models to be constructed and one which was used extensively from 1960-64 was Johnson's teardrop model (JOHNSON, 1960). The configuration, as shown in Figure 15, was determined by considering a supersonic flow past a spherical obstacle. The rate at which the flow can close behind the sphere is governed by the magneto-acoustic velocity, V_\perp . The tail length is given by (hV_s/V_\perp) , where h is a characteristic length along the polar axis. Using representative values, ($h \sim 15 R_E$, $V_s \sim 500$ km/sec, and $V_\perp \sim 70$ km/sec), the length is estimated to be $\sim (10)^2 R_E$.

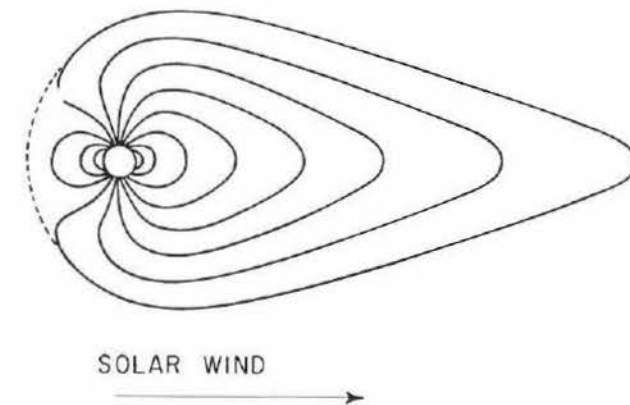


Fig. 15. Johnson's closed-tail teardrop model of the magnetosphere.

If you recall, the results of Pioneer 5 were interpreted initially to indicate an interplanetary field nearly perpendicular to the ecliptic plane (COLEMAN *et al.*, 1960). DUNGEY (1961) suggested that there would be two characteristically different configurations as a result of the possible interconnection of interplanetary and geomagnetic field lines. He argued that the interplanetary magnetic field merges with the geomagnetic field at the magnetopause whenever the interplanetary field has a component oppositely directed to the geomagnetic field. He further suggested that merging occurred on the sunlit side and the reverse takes place in the tail, where the temporary connection between the geomagnetic and interplanetary lines of force is broken.

Dungey's reconnection model is shown in Figure 16. The outer portion of the

geomagnetic field is merged with a Southward-directed interplanetary field. The interplanetary field and plasma close in behind the earth at the neutral sheet. The geomagnetic tail terminates at the neutral point with the interplanetary field and solar plasma beyond.

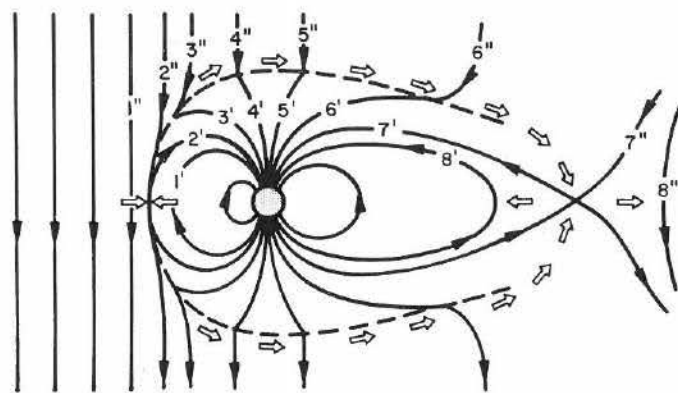


Fig. 16. Dungey's reconnection model of the magnetosphere.

Axford, Petschek and Siscoe modified Dungey's model to the form shown in Figure 17 (AXFORD *et al.*, 1965). The figure is topologically similar to Johnson's teardrop model and yet has some of the features of Dungey's reconnection model. Notice that there is no magnetic merging in the sunlit magnetopause; whereas in the tail, they incorporated the process of rapid annihilation at a neutral sheet due to Petschek.

The basic assumption for the reconnection model as well as for the Axford, Petschek, Siscoe model is that magnetic merging takes place. Whereas in a closed model it is assumed that magnetic merging in the presence of a highly conducting plasma is not an important process. As a result, a long, permanent geomagnetic tail is predicted.

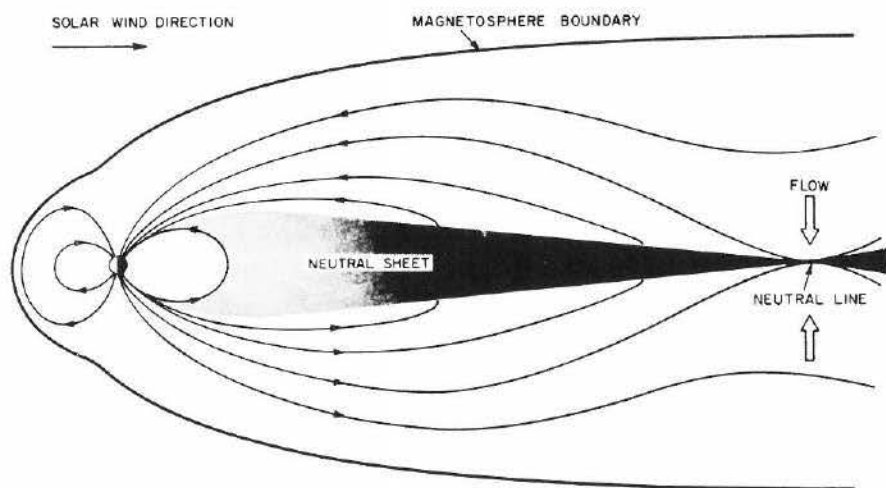


Fig. 17. Magnetospheric model by Axford, Petschek, and Siscoe.

Before discussing a magnetospheric model which incorporates the most recent data and interpretive ideas, let us outline the basic idea which is used in determining the shape of the magnetosphere. Consider a planar interface separating a uniform magnetic field and a normally incident neutral plasma (protons and electrons) traveling with a bulk velocity V_1 . We know that for equilibrium, there must be a pressure balance. Figure 18 gives the geometry of the problem under equilibrium conditions.

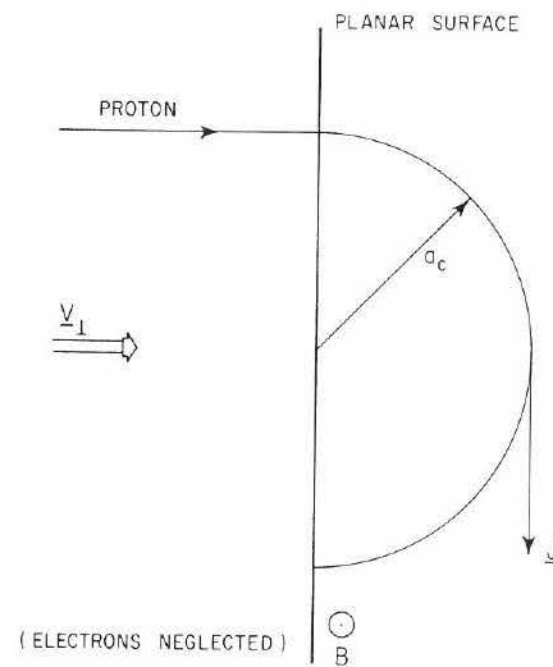


Fig. 18. Illustration of the pressure balance between a normally incident plasma and a uniform magnetic field at a planar interface.

We know that the repulsive force at the interface is produced by an induced current density, \mathbf{J} . Neglecting electrons, we see in Figure 18 that the protons in the plasma are deflected as they impinge on the magnetic field and follow a circular orbit. Here $a_c = MV_1/eB$ is the cyclotron radius for a proton. The net effect of these protons (and electrons) is to produce a current density \mathbf{J} normal to \mathbf{B} . If we neglect displacement currents, Maxwell's equation can be written as $\nabla \times \mathbf{B} = \mu_0 \mathbf{J}$. In terms of order of magnitudes, we have $B/L = \mu_0 N_e V$. In this case the characteristic length L is $2a_c$, so we obtain $B^2/2\mu_0 = NMV^2$. This equation tells us that equilibrium is achieved when the magnetic pressure equals the streaming plasma pressure. The current system is such that the magnetic field is zero on the plasma side of the surface and doubled inside. The amplification factor for the field depends on the geometry of the bounding surface. The factor 2 holds only for a plane. Thus, a 'balance' equation is used to determine the shape of the magnetosphere's bounding surface.

It is the solar-wind pressure that confines the geomagnetic field to some volume around the earth. The field in turn represents a blunt obstacle in the path of the supersonically flowing plasma. A bow shock is formed upstream of the earth's field because there is no signal which can propagate upstream in the unshocked wind to divert it around the obstacle (see Figure 19). Only after the wind is shocked and made subsonic can it flow around the obstacle.

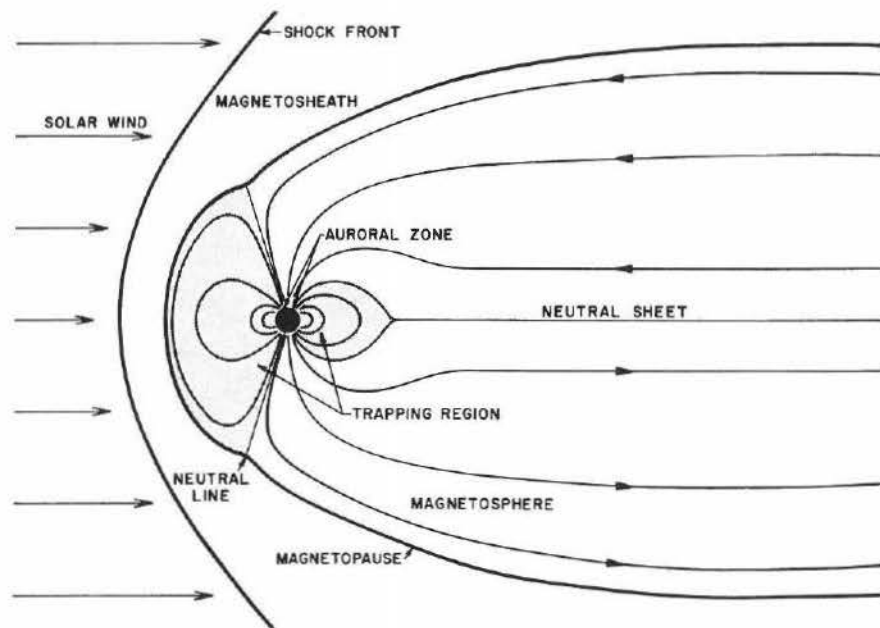


Fig. 19. Magnetospheric model with negligible merging.

The shock is said to be collisionless. Its thickness is of the order of the geometric mean of the proton and electron cyclotron radii (~ 10 km). In this short distance, the streaming energy of the solar wind is converted into thermal energy. Before there was any experimental evidence, there were speculations as to whether the electrons or protons would get the majority of the thermal energy. MICHEL (1965) argued on thermodynamic grounds (entropy considerations) that $T_i = T_e$, for weak shocks; and unless some special dissipative mechanism is in effect, this condition applies to strong shocks also.

The thick layer behind the bow shock is called the magnetosheath. The sheath part comes from the idea that a sheath is formed around spacecraft and meteors which enter the earth's atmosphere. As the interplanetary field lines are swept into this region by the flowing plasma they tend to pile up against the magnetosphere. The thickness of the magnetosheath is determined by the rate at which piled up field lines can slip around the magnetosphere.

The subsonic plasma in the nose region continues its journey around the sides of the magnetosphere. It expands and, at some point downstream, becomes supersonic.

Now the boundary between the shocked thermalized plasma and the earth's field is called the magnetopause in analogy with a boundary layer between regions in the atmosphere. The magnetosphere is contained by the magnetopause. It is filled with a tenuous gas of the earth's outer atmosphere and probably some solar-wind gas. There are two trapping regions; one persistent, the other short-lived. In the anti-solar direction, the magnetosphere stretches out to form a long tail.

Let us examine two mathematical determinations of the shape of the magnetosphere. Figure 20 compares boundaries as determined by IMP I with the theoretical predictions of Spreiter and Jones (NESS *et al.*, 1964; SPREITER and JONES, 1963). The results are shown in the ecliptic plane. The analytical determination of the magnetopause was obtained by assuming specular reflection of the solar wind off of the geomagnetic field. The location of the bow shock was calculated from a simple aerodynamic analogy. Agreement between prediction and observation is very good in the vicinity of the nose. Further back on the flanks the difference between observation and prediction increases. This deviation is caused by the fact that Spreiter and Jones were calculating the teardrop model with a tail that closes at $(10)^2 R_E$.

The magnetic data points shown were obtained from satellite traversals of the boundaries. On a typical out-bound orbit, the magnetic field decreases smoothly until the outer boundary is reached. Here there is a sharp decrease in field strength and a

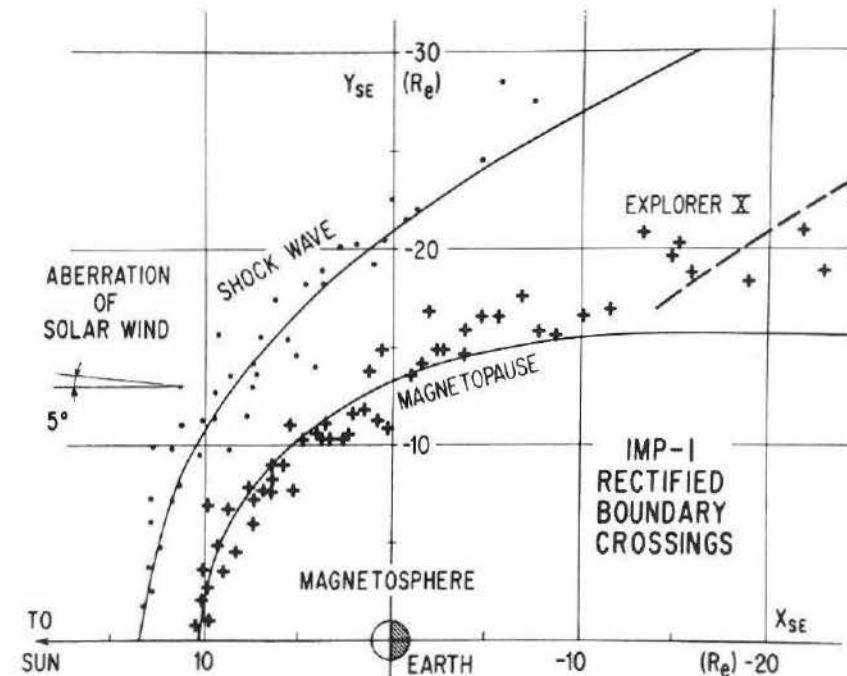


Fig. 20. The boundary of the magnetosphere in the ecliptic plane. (After NESS *et al.*, 1964; SPREITER and JONES, 1963.)

weaker fluctuating magnetic field is observed until finally the shock is detected. Plasma measurements also define this region clearly.

When this boundary determination was made, there were (and still are) many good theoretical reasons for assuming a long tail. Both external and internal mechanisms were postulated. For example, it is conceivable that the solar wind exerts a small but effective tangential drag on the magnetopause which results in its having a long cylindrical shape. This is an external mechanism. As an example of an internal mechanism, consider hydromagnetic waves which propagate down the tail in the anti-solar direction. The amplitude of these waves will grow until a hydromagnetic shock is formed which will blow the tail open. Once this happens, and in the absence of very rapid merging, it is very difficult to see how the tail could close in any short distance.

Detailed magnetic measurements made on IMP I showed that at distances of $30 R_E$, in the anti-solar direction, the magnetic lines of force are approximately parallel to the earth-sun line with a neutral sheet of no more than a few hundred kilometers thickness between regions of opposite fields (NESS *et al.*, 1964).

In order to understand and interpret trapped particle data, it is necessary to have an analytical representation of the magnetic field. For this reason, WILLIAMS and MEAD (1965) constructed a model of the magnetosphere that contained a neutral sheet. To account for a neutral sheet at about $10 R_E$, they calculated a field due to a current sheet in the tail and vectorially added this field to the dipole field as deformed by the solar wind. The resulting configuration causes the magnetosphere to be divided

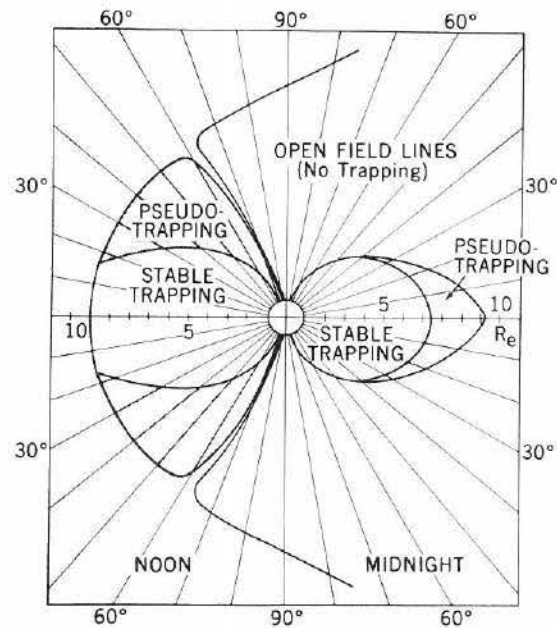


Fig. 21. Boundary in the noon-midnight meridional plane. (After ROEDERER, 1967.)

into regions of stable and pseudo-trapping as shown in Figure 21. The general effect is to stretch out the field on the dark side. Lines of force at high latitudes are not closed. They also stretch out into the tail and there is no trapping.

Today there is a general acceptance that the geomagnetic tail is very long, although at distances of $\sim(10)^3 R_E$, it appears to be breaking up into filaments. The field lines which enter the tail are determined by the location of the neutral points. The two neutral points on the sunlit side were first calculated by CHAPMAN and FERRARO (1940). They are in the noon-meridian. In the other meridional planes, there are points on the magnetopause that are analogous to the neutral points and these form a 'demarcation line' (WALTERS, 1966). Unlike the neutral point (zero field), each demarcation point does have a magnetic field. The field lines at latitudes less than the demarcation point latitudes tend to co-rotate with the earth. The lines at higher latitudes extend into the tail and we shall discuss them in a moment. The locus of all demarcation points defines the demarcation line which passes through the neutral point. The two demarcation lines are shown in Figure 22. Notice that the field directions on either side of the demarcation line are distinctly different and it is only at the neutral point that they are precisely oppositely directed.

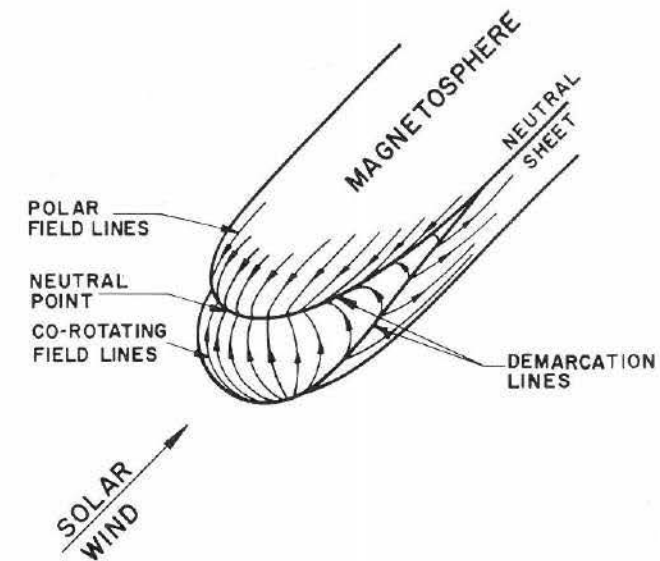


Fig. 22. Sketch of the demarcation lines.

The tail is defined by the two tubes of flux that emerge from the polar caps (latitudes greater than the demarcation-line latitude). Figure 23 is a sketch of how the field lines behave as they stretch out in the tail. The 24-hour rotation of the earth causes the spiral structure. The wavelength of the spiral has been estimated to be in the range $4(10)^2 R_E < \lambda < 7(10)^3 R_E$ (DESSLER and JUDAY, 1965).

Let us now look down the tail in an anti-solar direction and examine the angle that the neutral sheet makes with the plane of the ecliptic. The earth's spin axis is inclined

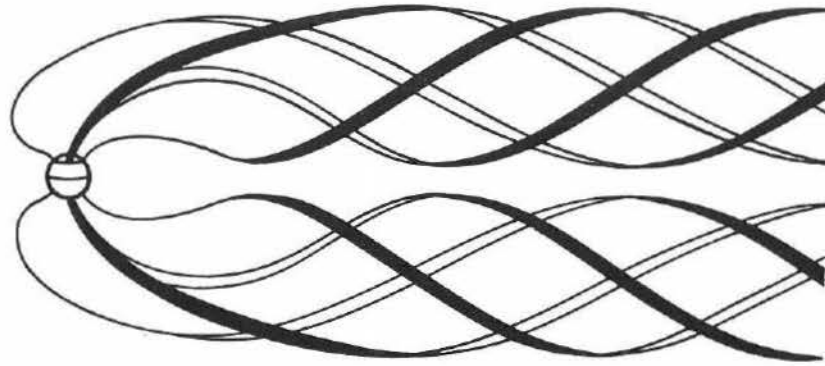


Fig. 23. Sketch of the behavior of auroral-zone field lines.

at $\sim 23^\circ$ to the ecliptic plane; while the dipole axis is inclined at $\sim 11^\circ$ with respect to the spin axis. So at extreme times for the proper day the angle of tilt could be as much as 34° . A summary of the tilting angle is given in Figure 24 (DESSLER and JUDAY, 1965).

The oblique angle made by the interplanetary magnetic field with the radially expanding solar wind results in an Easterly deflection of the solar wind as it passes the bow shock upstream of the geomagnetic field (WALTERS, 1964). We expect that this asymmetry will disappear in the distant tail because the influence of the shock is strong only in the nose region. The earth's orbital velocity relative to the radial solar-wind velocity vector also produces a deflection. The total deflection should be of the order of 10° .

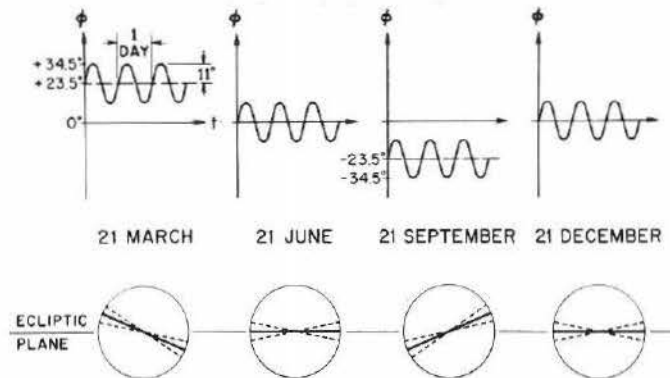


Fig. 24. Graphical representation of the centerline tilt angle.

The asymmetry is shown greatly exaggerated in Figure 25. The interplanetary field is shown at the Archimedean spiral angle and is excluded from the magnetosphere. It has slipped over and under the magnetopause. The interplanetary field exerts a pressure on the tail and we expect at large distances ($\lesssim (10)^2 R_E$) that the tail is flattened considerably.

3. Magnetic Disturbances

When we speak of magnetic activity we are referring to magnetic perturbations as they are observed on the earth's surface, viz., magnetic storms and micropulsations. These perturbations and phenomena associated with them derive their energy from the solar wind. The mechanism for energy transport across the magnetopause is not well understood and we shall not discuss it.

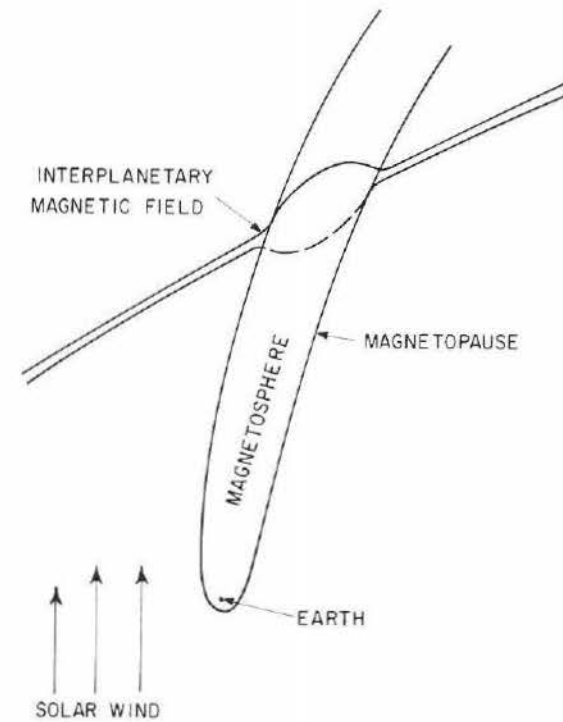


Fig. 25. The configuration of the magnetosphere and the interplanetary field.

Consider the magnetogram (of a magnetic storm) shown in Figure 26. It was taken at a low-to-mid-latitude observatory in Honolulu and covers a period of 3 days. The H , Z , and D traces represent the horizontal and vertical components, and the declination, respectively. The straight horizontal line shown is called the base line and observed departures from it and fluctuations with respect to it represent the magnetic activity.

Let us focus our attention on the horizontal component (H). At about 0145 (Honolulu time) there is a jump of about 20–30 γ in the field. It remains at this level for about an hour. Next we see H decrease to about 100 γ below the base line value as we enter into the main phase of the storm. Notice in particular the fluctuations that are occurring during this active period of time. They have a characteristic period which is somewhere between 20–40 min. Because of the large period, it is unlikely that

they are produced by hydromagnetic resonances in the magnetosphere. Such resonances have periods of the order of a minute or less. They are probably caused by the structure in the solar wind. Finally we see the slow recovery phase with the components returning ultimately to prestorm values.

We refer to magnetic fluctuations of this type as magnetic noise. It is often seen in the absence of a magnetic storm which suggests that it is caused by solar wind structure. There is also experimental evidence to corroborate this point of view.

Recall in the second lecture we discussed the sector structure of the solar wind observed by WILCOX and NESS (1965) (see Figure 5). The sectors are sharply bounded. Between the oppositely directed field lines there is a stable neutral sheet.

Sector properties for a period of 8 days are given in Figure 10. The observations

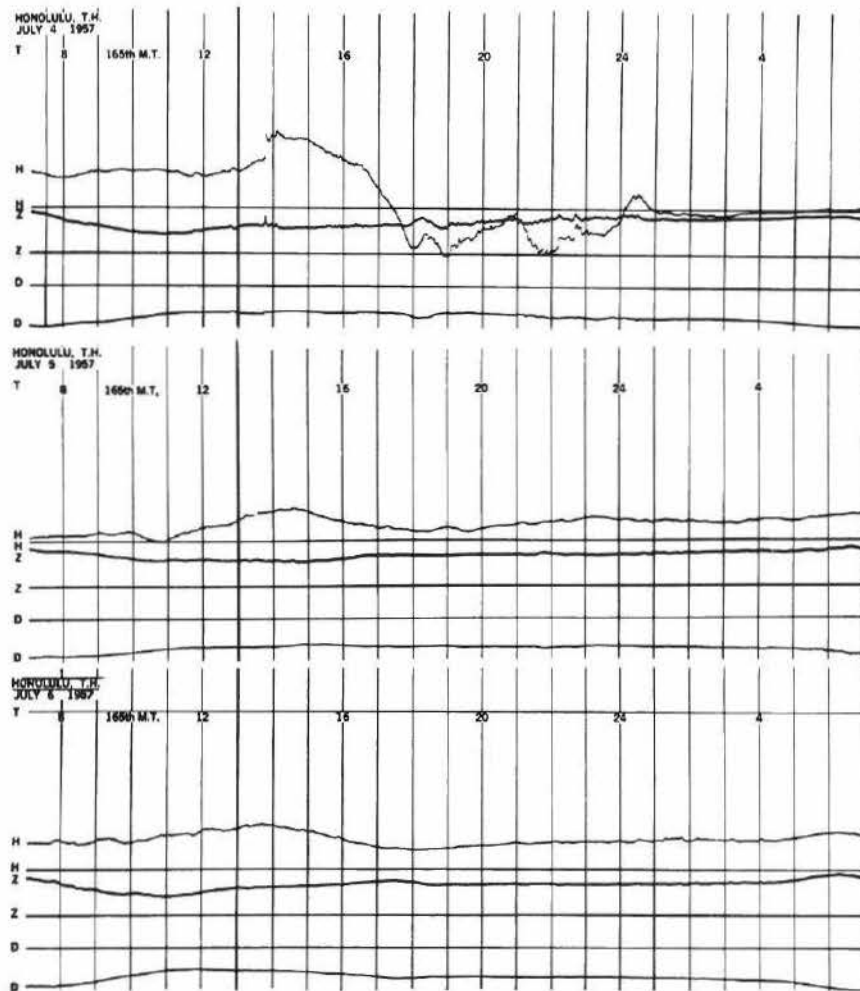


Fig. 26. A sample magnetic storm as observed at Honolulu.

were made during sunspot minimum and there was not much magnetic activity. We see that as a sector boundary is crossed the solar-wind density is rising and reaches a maximum in about a day; it then begins to decrease and finally it recovers and returns to nearly its initial value. The point is that the geomagnetic activity, although lagging the solar wind density by a day, exhibits a similar behavior.

There are two models at our disposal for explaining magnetic activity. They are shown in Figure 27. The lower one is Dungey's reconnection model which we discussed in the last lecture. The upper one is the non-merging model (DESSLER, 1964).

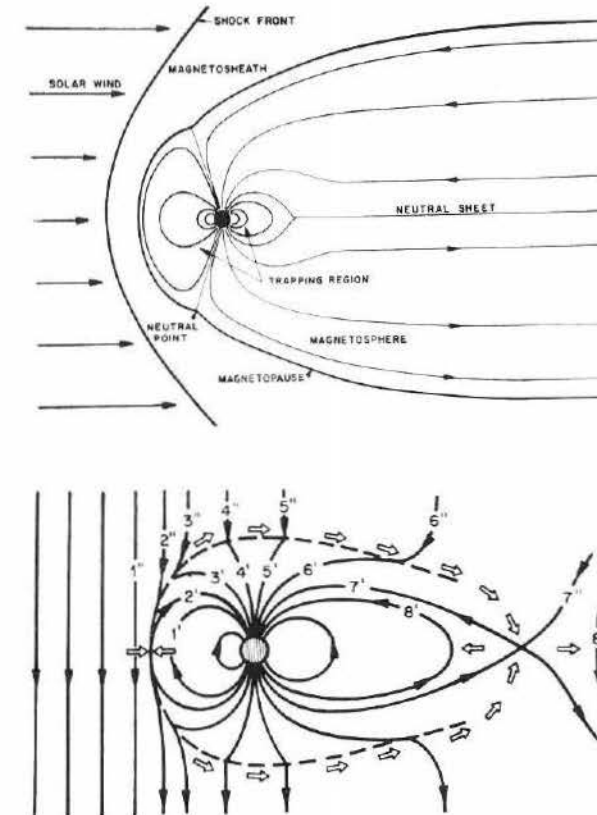


Fig. 27. Magnetospheric models: (a) Magnetic merging is negligible (after Dessler), (b) Appreciable merging (after Dungey).

Now the interplanetary field is in the plane of the ecliptic and makes an angle of 45° with respect to the earth-sun line. But this is not to say that it does not fluctuate up and down and back and forth. In the Dungey model, we expect increased magnetic activity when the field has a Southerly component and relative magnetic quiet when it has a Northerly one. On the other hand, in the non-merging model we expect K_p to be independent of the direction of the interplanetary magnetic field.

Measurements made on IMP 3, and as reported by Wilcox and Ness, are shown in Figure 28. Here K_p is plotted against θ , the angle that the interplanetary field makes with respect to the ecliptic plane. With this amount of data it is possible to extract some information out of the noise by using statistical techniques. Each heavy dot is representative of 1/10 of the total data chosen and weighted properly. It is clear from these results that as K_p decreases the field component changes from a Southward to a Northward one. Figure 29 shows the same general result. Only here the field strength is plotted against K_p . Again we see the sloping average which agrees with Dungey's expectation.

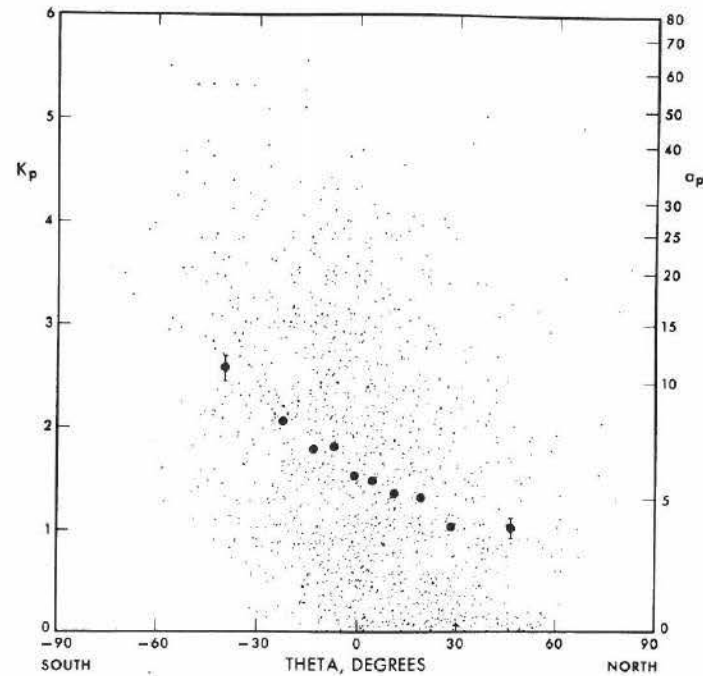


Fig. 28. Magnetic activity plotted against the angle that the interplanetary magnetic field makes with respect to the ecliptic plane.

In an earlier lecture we discussed the possibility of a faster solar wind overtaking a slower plasma as the sun rotates (cf. Figure 14). The collision of these plasmas leads to the formation of two shock waves and a tangential velocity discontinuity between them. We expect the magnetic field and plasma to be irregular and disturbed between the two shock waves. Now if this portion of the solar wind has a time dependent structure when it pushes on the magnetosphere, it will modulate the size of the cavity. Thus we can think of the magnetopause as 'breathing in and out' and generating hydromagnetic waves that propagate inward. This picture of the interaction gave rise to the interpretation that K_p is a measure of the time rate of change of the sum of plasma and magnetic pressure acting on the magnetosphere (DESSLER and FEJER, 1963).

The question arises as to how the large-scale, low-frequency magnetic irregularities in the magnetosheath should be interpreted. Similar irregularities are not observed within the magnetosphere; they appear suddenly as the magnetopause is crossed (CAHILL and AMAZEEN, 1963; HEPPNER *et al.*, 1963). If the irregular fluctuations are hydromagnetic waves then the impedance mismatch for wave propagation across the magnetopause into the magnetosphere must be very great.

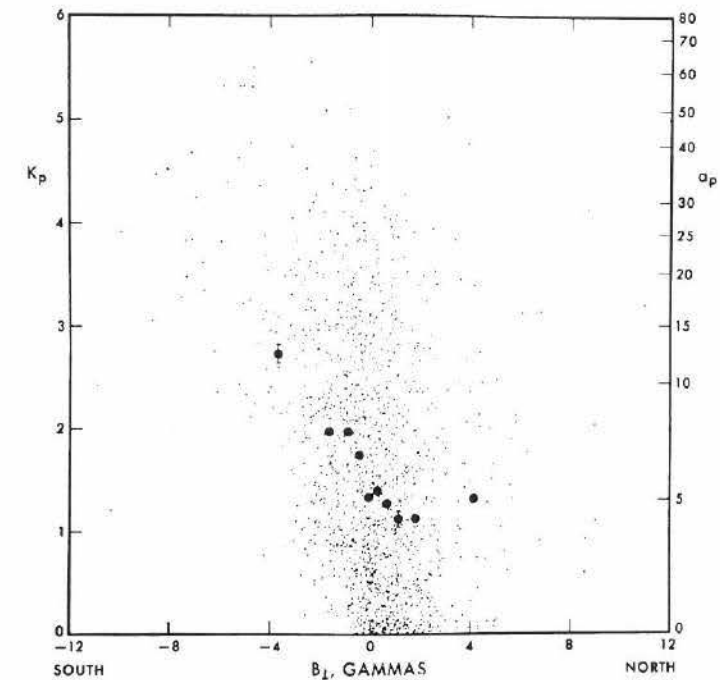


Fig. 29. Magnetic activity plotted against the normal component of the interplanetary magnetic field.

Fejer has shown that at a velocity discontinuity of the type presented by the magnetopause, only one of the three possible types of waves, the Alfvén wave, cannot penetrate the interface (FEJER, 1963). The modified Alfvén and sound waves penetrate freely into the magnetosphere unless the density in the magnetosheath is much larger (factor of 10 or more) than the density in the magnetosphere. Even in this case, waves which are normally incident (or nearly so) are transmitted. Thus it is hard to explain the almost total absence of fluctuations within the magnetosphere if we have hydro-magnetic waves in the magnetosheath.

If all three types of waves exist in the magnetosheath we should expect the magnetopause to be distorted or rippled by these waves. Then there would be some wave transmission into the magnetosphere but most of these waves would be evanescent and penetration would only occur to distances smaller than one wavelength. This kind of perturbation is represented by a dotted curve in Figure 30. Such waves were not

observed by CAHILL and AMAZEEN (1963) on Explorer 12. Therefore, we may conclude that the observed irregularities in the magnetosheath are not hydromagnetic waves; they must be quasi-static structure in the field that is swept along by the solar wind. Furthermore, the sum of plasma and magnetic pressure must be constant throughout the irregularities because any non-uniformity in total pressure would either propagate as a wave or wrinkle the surface of the magnetosphere.

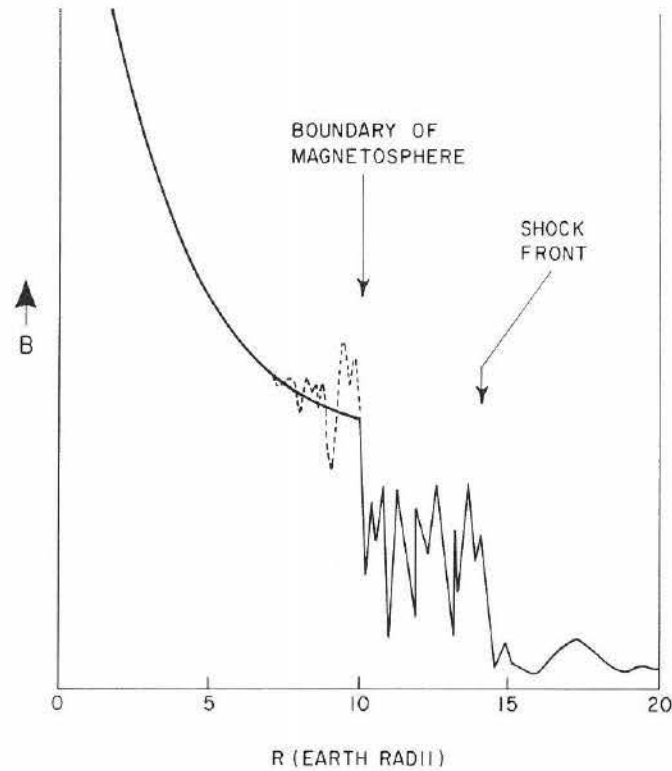


Fig. 30. Magnetic profile of a boundary crossing with superposed hydromagnetic wave perturbations shown in dotted curve.

Mariner 2 data showed that a positive relationship exists between solar-wind velocity and the daily sum of the geomagnetic index (ΣK_p) (SNYDER *et al.*, 1963). As we can see from Figure 31, there is a large scatter and again the correlation is weak.

There is no strong correlation between the size of the magnetopause, as determined by satellite crossings, and geomagnetic-activity indices (PATEL and DESSLER, 1966). The data were obtained from Explorer 12 and IMP I. For purposes of comparison, the boundary crossings were reduced to the equivalent distance that would have resulted, had all measurements been made at the stagnation point. Latitude corrections were made using the factor $(1 + 3 \sin^2 \lambda_s)^{1/6}$, where λ_s is the geomagnetic latitude to the subsolar point (NESS *et al.*, 1964). A longitudinal correction was made using magnetospheric boundary traces calculated by MEAD and BEARD (1964).

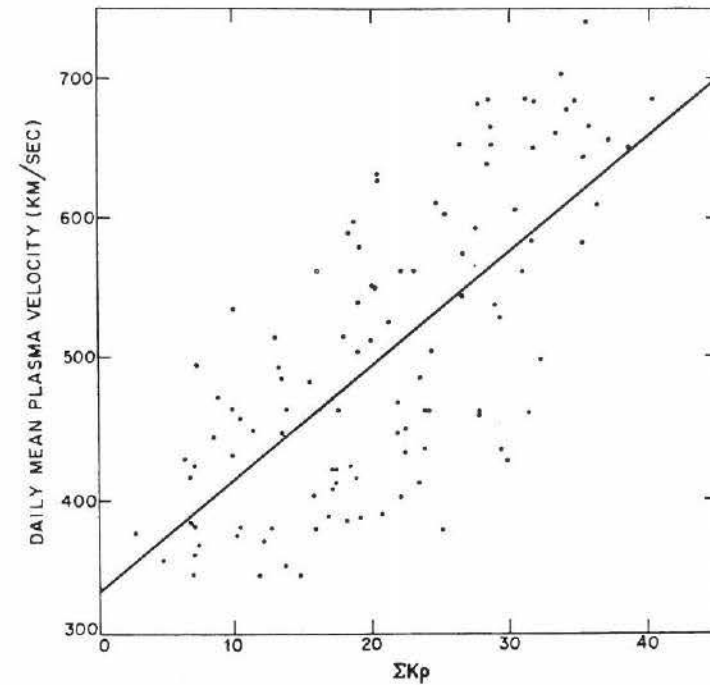


Fig. 31. The daily mean plasma velocity versus ΣK_p .

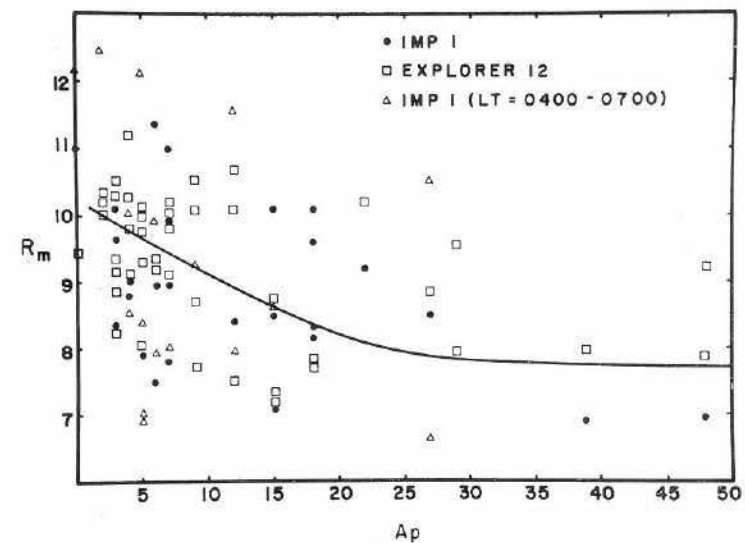


Fig. 32. Magnetopause distance to the subsolar point versus A_p .

A scatter diagram showing normalized magnetopause distances R_m and geomagnetic activity is given in Figure 32. Three-hour a_p values that contain the time of magnetopause crossings are used. No clear correlation is evident although data for a large range of R_m and a_p are shown. A weak inverse relationship between R_m and a_p may be present but the scatter is too large to support such a conclusion.

Small values of R_m ($7-8 R_E$) can occur during periods of magnetic quiet. This indicates that magnetic quiet can occur during periods of high solar-wind momentum pressure. The large spread in R_m for small values of a_p can be explained in part by Freeman's data which showed that the magnetopause distance was large during the recovery phase of a magnetic storm (FREEMAN, 1964). This he explained as being due to the distortion of the magnetosphere by the internal pressure of the main phase ring current during the recovery phase when magnetic indices are generally low.

4. Field-Aligned Current Systems

Let us now turn to another topic – field-aligned current systems, a concept first suggested by BIRKELAND (1908). Consider two observatories thousands of kilometers apart. Sometimes magnetic variations with periods of a few minutes are observed at them simultaneously; at other times there are essentially no similarities in the magnetograms. An example is shown in Figure 33 for Fredericksburg, Va. and Tucson, Ariz. The records are very similar between 0330 and 0430 UT and there is a gross difference during the time interval between 0500 and 0600 UT.

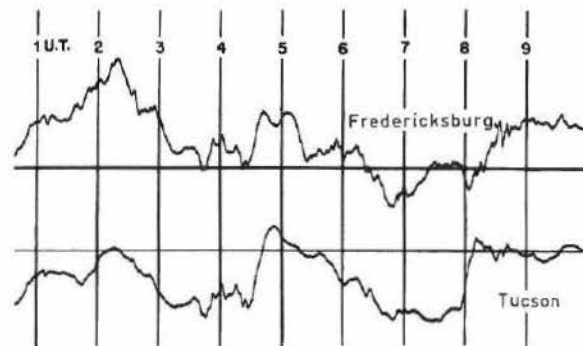


Fig. 33. Horizontal component of the earth's field versus time from the Fredericksburg and Tucson magnetic observatories.

Similar world-wide fluctuations in the magnetic field are probably well explained in terms of hydromagnetic waves propagating through the magnetosphere because here the wavelength is so large (of the order of the size of the magnetosphere) that it affects the whole earth almost simultaneously. For localized fluctuations however, such an interpretation is not possible. In this case, the fluctuations are better interpreted in terms of field-aligned currents in the magnetosphere.

Figure 34 is a sketch showing how a hydromagnetic wave might be propagated

along the earth's field lines from the equator by means of several successive total internal reflections from a field-aligned density discontinuity. For propagation in a wave guide, the minimum transverse dimension must be approximately equal to the wavelength (BOOKER, 1962). For the type of guidance illustrated in Figure 34 the wave cannot be confined to a dimension smaller than $\lambda/4$.

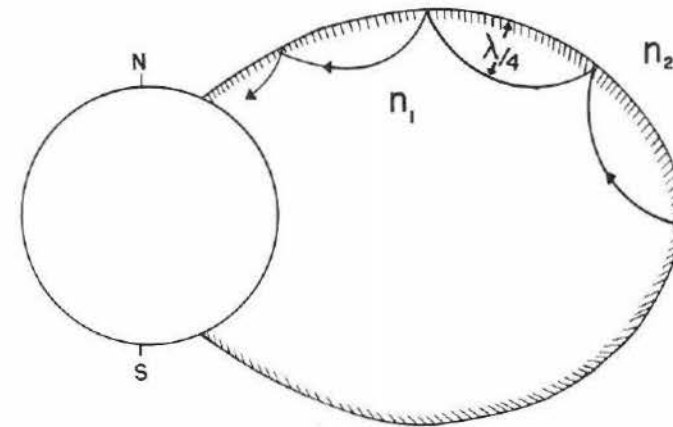


Fig. 34. Sketch of how a hydromagnetic wave might be propagated along a field line by means of successive total internal reflections.

Suppose we try to explain the shortest period reported (~ 10 sec) as being guided within the largest dimension reported (~ 400 km) (ZMUDA *et al.*, 1966). Figure 35 shows the wavelength λ of a hydromagnetic wave with a 10-sec period at an altitude of 1000 km near the auroral zone for a wide range of ionospheric number density and

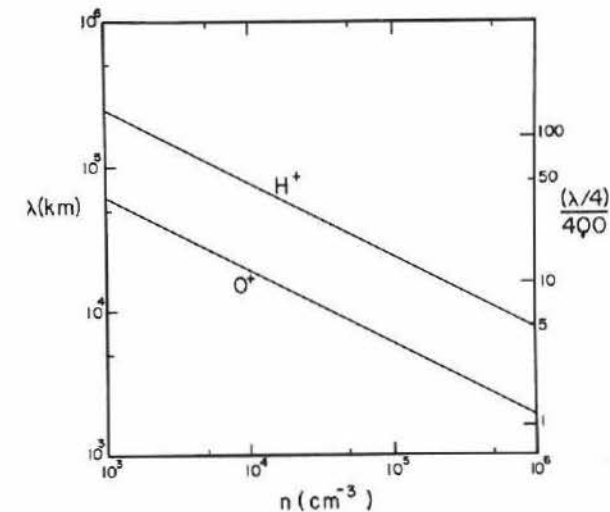


Fig. 35. Wavelength of a hydromagnetic wave with a 10-sec period as a function of ion density.

composition. The right ordinate gives the ratio of a quarter wavelength to the largest dimension observed showing the magnetic fluctuations (400 km). Even if we were to assume a pure oxygen ionosphere with a number density of $(10)^5/\text{cm}^3$, we see that $(\lambda/4)$ is four times the maximum 400 km dimension. For less favorable assumptions the wavelength becomes comparable with the dimensions of the magnetosphere itself, and the observed confinement is hundreds of times smaller than $\lambda/4$. It is evident that we can not obtain a fit to the minimum criteria.

Thus it is reasonable to assume that the long-period (≥ 60 sec) localized perturbations are due to quasi-static field-aligned current systems. Field-aligned currents are produced by charge separation and there are a variety of mechanisms for inducing charge separation. We shall consider the flute instability. As we know from whistler investigations there is a marked change in number density as we cross the outer boundary of the plasmasphere. Let us idealize this situation and assume we have a plasma-vacuum interface as shown in Figure 36. The interface is immersed in a magnetic field that has a gradient normal to the lines of force. The lines of force are parallel to the interface and the surface is perturbed with a fluted boundary. The drift motion of the charged particles induced by the gradient in the magnetic field causes a periodic build up of charge on the boundary and the resultant crossed-fields drift motion causes the fluted boundary to become more fluted. In this way, a potential difference between field lines is established (CUMMINGS and DESSLER, 1967). Now conductivity parallel to the field lines is very high, and for quasi-static conditions the field lines may be considered to be equipotential lines. Thus we expect current to flow down the field lines, to be shorted across the ionosphere, and then to flow up the field lines to complete the circuit. The geometry of the system is shown in Figure 37. Such a system may well be responsible for localized magnetic disturbances.

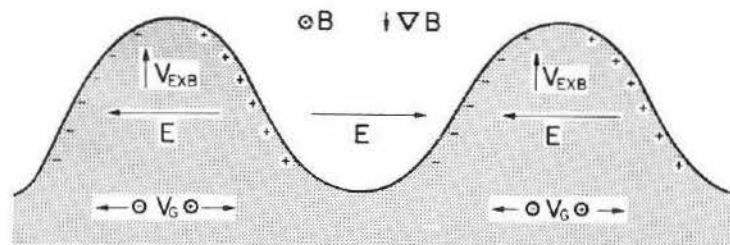


Fig. 36. Schematic representation of the flute instability.

The strength of the electric fields associated with the flute instability depends on the ionospheric Pederson conductivity. For example, if the ionospheric Pederson conductivity is infinite, the flute-instability electric fields will be shorted out, and any flute structure that develops will be stabilized.

The energy made available by the flute instability may be dissipated in the ionosphere as Joule heat from the stabilizing currents. This heating mechanism could deposit enough heat into the ionosphere during a magnetic storm to compete with the

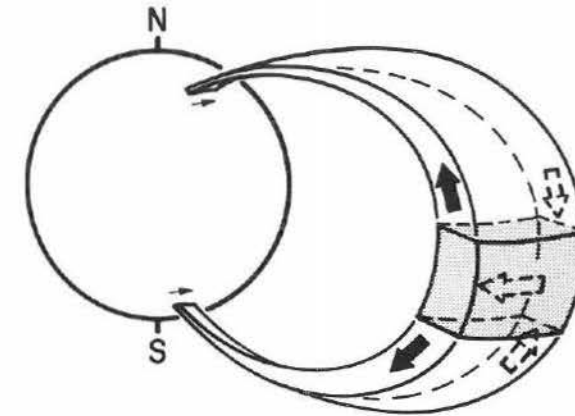


Fig. 37. Schematic representation of a field-aligned current system.

normal solar UV heat input and thus contribute to storm-correlated increases in satellite drag (CUMMINGS and DESSLER, 1967).

The last topic that we shall examine in this series of lectures is the interaction of the solar wind and the moon. Earlier we discussed the correlation of magnetic activity and solar-wind velocity (SNYDER *et al.*, 1963). We might expect that when a body such as the moon is at or near inferior conjunction, the solar wind flow will be disturbed and could, thereby, affect the geomagnetic field (MICHEL *et al.*, 1964). Whether the effect will be detectable or not is an entirely different matter. Figure 38 shows to scale the relative size and position of parameters expected to be important to any geomagnetic

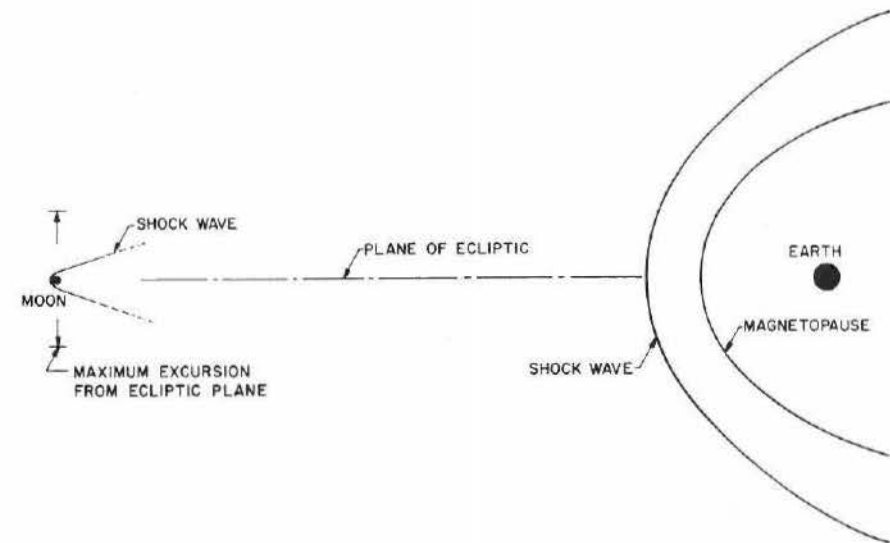


Fig. 38. Relative size and dimensions of the earth-moon system showing the approximate position of the magnetopause and standing bow shock.

effects from the moon. Notice that even though the moon's orbit is inclined to the ecliptic, its wake, if any, should always sweep across the magnetosphere at new moon.

Using K_p data from 1932 to 1964, the variation of geomagnetic activity with the phase of the moon has been tested for statistical significance (RASSBACH *et al.*, 1966). The fluctuations in K_p at the lunar period are typical of the periods near it, and in fact are within one standard deviation of the average fluctuation amplitude. The K_p fluctuations are due to the sun. The 27-day peak due to the sun has a width of about 7 days so that it is broad and contributes to periods between 24 and 31 days. Any narrow-band detection system, such as the superposed epoch analysis, senses the solar effect anywhere within this broad interval and the 29.5-day lunar period certainly falls within this interval. When the non-random variation in K_p caused by the broad solar peak is included in the analysis, the lunar effect falls well within the limits of chance occurrence. Thus we may conclude that available data do not indicate any statistically significant lunar influence on geomagnetic activity; the effect at 29.53 days periodicity that has been attributed to the moon is actually due to the sun.

Let us conclude the lecture by discussing conditions such that there will be a standing shock in front of the moon. The interplanetary magnetic field is frozen in the solar wind, and, as it flows past the moon, the field will pile up against the moon if its conductivity is higher than some critical value. This condition is shown in Figure 39. The critical value of conductivity for which the solar magnetic field will begin to pile up on the sunward side of the moon is given by equating the time for the magnetic-field lines to diffuse through the moon with the time for the solar-wind plasma to flow past the moon. The diffusion time is $t_D = \mu_0 \sigma R_M$, where R_M is the lunar radius; and the time for the solar plasma to flow past the moon is $t = R_M / V_S$. Setting $t_D = t$,

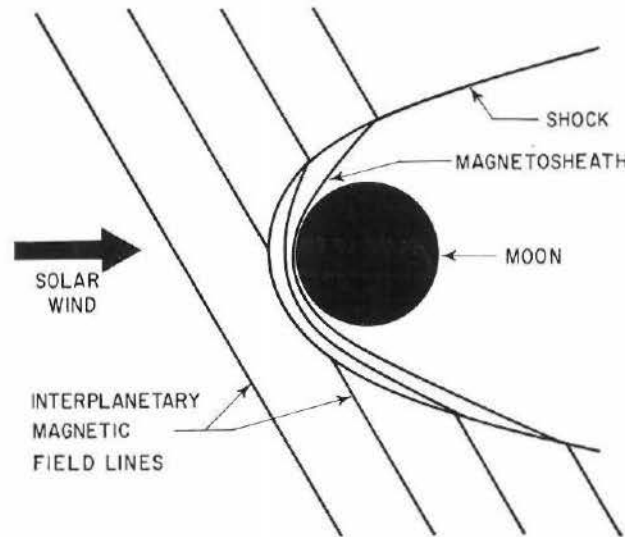


Fig. 39. Illustration of a possible bow shock formed by the interaction between the solar wind and the moon.

we obtain

$$\sigma_c = (1/\mu_0 R_M V_S). \tag{17}$$

To demonstrate this effect, consider a cube of conductivity σ and of length l on an edge, being placed in the solar wind, as shown in Figure 40. Since both the cube and the solar wind are conducting, a current, $J = \oint j \cdot ds$, flows through the cube. Since $j = \sigma E$, and from the hydromagnetic approximation, $E = -V_S \times B$, we have

$$J = \sigma V_S B_{\perp} l^2. \tag{18}$$

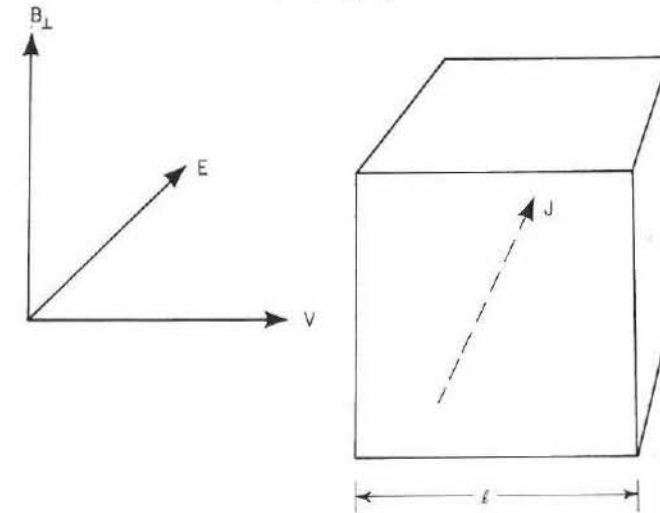


Fig. 40. The interaction of a conducting body with a streaming, highly conducting, uniformly magnetized plasma.

We can relate the magnetic field near the surface of the cube to the current flowing within it by using Maxwell's equation in integral form. Thus, $\oint B_J \cdot dl = \mu_0 \oint j \cdot ds$ gives

$$4lB_J = \mu_0 J, \tag{19}$$

where B_J is the field due to current flowing through the cube.

We are interested in the case where the magnetic field is doubled just ahead of the cube and zero behind it, i.e., $B_J \sim B_{\perp}$. Under this condition, Equations (18) and (19) yield

$$(l/V_S) = (\mu_0 \sigma l^2 / 4) \sim \mu_0 \sigma l^2, \tag{20}$$

where (l/V_S) is the time for the solar wind to sweep past the cube and $\mu_0 \sigma l^2$ is the time for the magnetic field to diffuse through the cube. If we let $l = R_M$, Equation (20) determines the critical conductivity.

Thus as long as the moon's conductivity is great enough so that the current J can flow through it, the magnetic-diffusion time through it is longer than the time for the solar wind to flow past, and the magnetic field will 'pile up' in front of it. In this way, we produce a standing shock as shown in Figure 39. However, if something impedes the current (such as a non-conducting dust layer) there will be no field pile up, and no shock, no matter how high the interior conductivity.

References

- ALFVÉN, H.: 1947, Granulation, Magneto-Hydrodynamic Waves, and the Heating of the Solar Corona, *Monthly Notices Roy. Astron. Soc.* **107**, 211–219.
- AXFORD, W. I., PETSCHKE, H. E., and SISCOE, G. L.: 1965, Tail of the Magnetosphere, *J. Geophys. Res.* **70**(5), 1231–1236.
- BIERMAN, L.: 1946, Zur Deutung der chromosphärischen Turbulenz und des Exzesses der UV-Strahlung der Sonne, *Naturwiss.* **33**, 118–119.
- BIERMAN, L.: 1951, Kometenschweife und solare Korpuskularstrahlung, *Z. Astrophys.* **29**, 274–286.
- BIERMAN, L.: 1953, Physical Processes in Comet Tails and their Relation to Solar Activity, *Mem. Soc. Roy. Sci. Liege Quatr. Ser.* **13**, 291–302.
- BIERMAN, L.: 1957, Solar Corpuscular Radiation and the Interplanetary Gas, *Observatory* **77**, 109–110.
- BIRKELAND, Kr.: 1896, Sur les rayons cathodiques sous l'action de forces magnétiques intenses, *Arch. Sci. Phys. Naturelles* **1**, 497–512.
- BIRKELAND, Kr.: 1908, *The Norwegian Aurora Polaris Expedition 1902–3*, vol. 1: *On the Cause of Magnetic Storms and the Origin of Terrestrial Magnetism*, first section, H. Aschehoug and Co., Christiania.
- BOOKER, H. G.: 1962, Guidance of Radio and Hydromagnetic Waves in the Magnetosphere, *J. Geophys. Res.* **67**, 4135–4162.
- CAHILL, L. J. and AMAZEEN, P. G.: 1963, The Boundary of the Geomagnetic Field, *J. Geophys. Res.* **68**, 1835–1843.
- CHAMBERLAIN, J.: 1960, Interplanetary Gas, 2: Expansion of a Model Solar Corona, *Astrophys. J.* **131**, 47–56.
- CHAPMAN, S.: 1918, The Energy of Magnetic Storms, *Monthly Notices Roy. Astron. Soc.* **79**, 70–83.
- CHAPMAN, S.: 1919, An Outline of a Theory of Magnetic Storms, *Proc. Roy. Soc. London A95*, 61–83.
- CHAPMAN, S.: 1929, Solar Streams of Corpuscles: their Geometry, Absorption of Light, and Penetration, *Monthly Notices Roy. Astron. Soc.* **89**, 456–470.
- CHAPMAN, S. and FERRARO, V. C. A.: 1931, A New Theory of Magnetic Storms, *Terrest. Magnetism Atmospheric Elec.* **36**, 77–97.
- CHAPMAN, S. and FERRARO, V. C. A.: 1940, The Theory of the First Phase of a Geomagnetic Storm, *Terrest. Magnetism Atmospheric Elec.* **45**, 245–268.
- CLAUSER, F. H.: 1960, The Aerodynamics of Mass Loss and Mass Gain of Stars. Johns Hopkins University Lab. Rept. AFOSR TN 60-1386, Nov.
- COLEMAN, P. J., Jr., DAVIS, Jr., L., SMITH, E. J., and JONES, D. E.: 1966, Variations in the Polarity Distribution of the Interplanetary Magnetic Field, *J. Geophys. Res.* **71**, 2831–2839.
- COLEMAN, P. J., Jr., DAVIS, Jr., L., SMITH, E. J., and SONETT, C. P.: 1962, Mariner 2: Interplanetary Magnetic Fields, *Science* **138**, 1099–1100.
- COLEMAN, P. J., Jr., DAVIS, L., and SONETT, C. P.: 1960, Steady Component of the Interplanetary Magnetic Field: Pioneer V, *Phys. Rev. Letters* **5**, 43–46.
- CUMMINGS, W. D. and DESSLER, A. J.: 1967, Field-Aligned Currents in the Magnetosphere, *J. Geophys. Res.* **72**, 1007–1013.
- DESSLER, A. J.: 1964, Length of Magnetospheric Tail, *J. Geophys. Res.* **69**, 3913–3918.
- DESSLER, A. J.: 1967, Solar Wind and Interplanetary Magnetic Fields, *Rev. Geophys.* **5**, 1–41.
- DESSLER, A. J. and FEJER, J. A.: 1963, Interpretation of Kp Index and M-Region Geomagnetic Storms, *Planetary Space Sci.* **11**, 505–511.
- DESSLER, A. J. and JUDAY, R. D.: 1965, Configuration of Auroral Radiation in Space, *Planetary Space Sci.* **13**, 63–72.
- DUNGEY, J. W.: 1961, Interplanetary Magnetic Field and the Auroral Zones, *Phys. Rev. Letters* **6**, 47–48.
- FEJER, J. A.: 1963, Hydromagnetic Reflection and Refraction at a Fluid Velocity Discontinuity, *Phys. Fluids* **6**, 508–512.
- FITZGERALD, G. F.: 1900, Sunspots, Magnetic Storms, Comet Tails, Atmospheric Electricity and Aurorae, *The Electrician* **46**, 287–288.
- FREEMAN, J. W., Jr.: 1964, The Morphology of the Electron Distribution in the Outer Radiation

- Zone and near the Magnetospheric Boundary as Observed by Explorer 12, *J. Geophys. Res.* **69**, 1691–1723.
- GOLD, T.: 1959, Motions in the Magnetosphere of the Earth, *J. Geophys. Res.* **64**, 1219–1224.
- HEPPNER, J. P., NESS, N. F., SCEARCE, C. S., and SKILLMAN, T. L.: 1963, Explorer 10 Magnetic Field Measurements, *J. Geophys. Res.* **68**, 1–46.
- JOHNSON, F. S.: 1960, The Gross Character of the Geomagnetic Field in the Solar Wind, *J. Geophys. Res.* **65**, 3049–3051.
- KELVIN, W. T.: 1892, Address to the Royal Society at their Anniversary Meeting, Nov. 30, 1892, *Proc. Roy. Soc. London A52*, 300–310.
- MEAD, G. D. and BEARD, D. B.: 1964, Shape of the Geomagnetic Field Solar Wind Boundary, *J. Geophys. Res.* **69**, 1169–1179.
- MICHEL, F. C.: 1965, Nonthermal Properties of a Postshock Plasma, *Phys. Fluids* **8**(7), 1283–1287.
- MICHEL, F. C., DESSLER, A. J., and WALTERS, G. K.: 1964, A Search for Correlation between Kp and the Lunar Phase, *J. Geophys. Res.* **69**, 4177–4181.
- NESS, N. F.: 1966, Simultaneous Measurements of the Interplanetary Magnetic Field, *J. Geophys. Res.* **71**, 3319–3324.
- NESS, N. F. and WILCOX, J. M.: 1964, The Solar Origin of the Interplanetary Magnetic Field, *Phys. Rev. Letters* **13**, 461–464.
- NESS, N. F. and WILCOX, J. M.: 1965, Sector Structure of the Quiet Interplanetary Magnetic Field, *Science* **148**, 1592–1594.
- NESS, N. F., SCEARCE, C. S., and CANTANARO, S. C.: 1966, Preliminary Results from the Pioneer 6 Magnetic Field Experiment, *J. Geophys. Res.* **71**, 3305–3313.
- NESS, N. F., SCEARCE, C. S., and SEEK, J. B.: 1964, Initial Results of the IMP I Magnetic Field Experiment, *J. Geophys. Res.* **69**, 3531–3569.
- NEUGEBAUER, M. and SNYDER, C. W.: 1966, Mariner 2 Observations of the Solar Wind, 1: Average Properties, *J. Geophys. Res.* **71**, 4469–4484.
- PARKER, E. N.: 1958, Interaction of the Solar Wind with the Geomagnetic Field, *Phys. Fluids* **1**, 171–187.
- PARKER, E. N.: 1963, *Interplanetary Dynamical Processes*, Interscience Publishers, New York.
- PATEL, V. L. and DESSLER, A. J.: 1966, Geomagnetic Activity and Size of the Magnetospheric Cavity, *J. Geophys. Res.* **71**, 1940–1942.
- PATTERSON, T. N. L., JOHNSON, F. S., and HANSON, W. B.: 1963, The Distribution of Interplanetary Hydrogen, *Planetary Space Sci.* **11**, 767–778.
- PETSCHKE, H. E.: 1964, Magnetic Field Annihilation, in *AAAS-NASA Symp. on the Physics of Solar Flares* (ed. by W. N. Hess), NASA SP-50, pp. 425–437.
- RASSBACH, M. E., DESSLER, A. J., and CAMERON, A. G. W.: 1966, The Lunar Period, the Solar Period, and Kp, *J. Geophys. Res.* **71**, 4141–4146.
- ROEDERER, J. G.: 1967, On the Adiabatic Motion of Energetic Particles in a Model Magnetosphere, *J. Geophys. Res.* **72**, 981–992.
- SNYDER, C. W., NEUGEBAUER, M., and RAO, U. R.: 1963, The Solar Wind Velocity and its Correlation with Cosmic Ray Variations and with Solar and Geomagnetic Activity, *J. Geophys. Res.* **68**, 6361–6370.
- SPREITER, J. R. and JONES, W. P.: 1963, On the Effect of a Weak Interplanetary Magnetic Field on the Interaction between the Solar Wind and the Geomagnetic Field, *J. Geophys. Res.* **68**, 3555–3564.
- WALTERS, G. K.: 1964, Effect of Oblique Interplanetary Magnetic Field on Shape and Behavior of the Magnetosphere, *J. Geophys. Res.* **69**, 1769–1783.
- WALTERS, G. K.: 1966, On the Existence of a Second Standing Shock Wave attached to the Magnetopause, *J. Geophys. Res.* **71**, 1341–1344.
- WILCOX, J. M. and NESS, N. F.: 1965, Quasi-Stationary Co-Rotating Structure in the Interplanetary Medium, *J. Geophys. Res.* **70**, 5793–5805.
- WILLIAMS, D. J. and MEAD, G. D.: 1965, Nightside Magnetosphere Configuration as Obtained from Trapped Electrons at 1100 Kilometers, *J. Geophys. Res.* **70**, 3017–3029.
- WURM, K.: 1943, Die Natur der Kometen, *Mitteilungen Hamb. Sternw. in Bergedorf* **8**, 57–92.
- ZMUDA, A. J., MARTIN, J. H., and HEURING, F. T.: 1966, Transverse Hydromagnetic Disturbances at 1100 Km in the Auroral Region, *J. Geophys. Res.* **71**, 5033–5045.